Fabrication and Characterization of Porosity-Gradient Poly lactic Acid/Bredigite Composite Scaffolds via Fused Deposition Modeling for Bone Tissue Engineering

Somayeh Mohammadi[1], Hamid Reza Rezaie[1*], Jafar Javadpour[2], Mahshid Kharaziha[3], Ali Reza Khavandi[4]

[1] Department of Materials and Metallurgical Engineering, Iran University of Science and Technology, Tehran, Iran.

[1*] Department of Materials and Metallurgical Engineering, Iran University of Science and Technology, Tehran, Iran.

[2]Department of Materials and Metallurgical Engineering, Iran University of Science and Technology, Tehran, Iran.

[3]Biomaterials Research Group, Department of Materials Engineering, Isfahan University of Technology, Isfahan, Iran.

[4]Department of Materials and Metallurgical Engineering, Iran University of Science and Technology, Tehran, Iran.

ABSTRACT

Despite extensive research on three-dimensional (3D)-printed scaffolds for bone tissue engineering, constructs capable of accurate replication of bone structure have remained a significant challenge. This study, aims to develop porosity-gradient scaffolds based on poly lactic acid (PLA)/Bredigite ($Ca_7MgSi_4O_{16}$) nanoparticles using the fused deposition modeling (FDM) technology to simulate the two distinct cortical and cancellous layers of the natural bone with 3-D interconnectivity to promote richer supply of blood, oxygen, and nutrients for healthy in-growth of bone cells and supporting mechanical properties necessary for tissue growth. The role of Bre nanoparticles and porosity gradient on the mechanical, physiological, and biological properties of scaffolds was also addressed. The results showed a significant improvement in the compressive strength of the scaffolds with porosity gradient compared to scaffolds without gradient (i.e. compressive strength of 172 ± 32.2 MPa for PLA/20% Bre scaffold vs. 40.2 ± 24 MPa for the pure polymer scaffold). The scaffolds with porosity gradient and Bre nanoparticles significantly improved the in vitro bioactivity of scaffolds, proliferation, osteogenic differentiation of osteoblast-like cells, and mechanical properties, making them attractive for bone regeneration. In summary, the PLA/Bre scaffolds with porosity gradient can be an appropriate candidate for bone tissue engineering.

KEYWORDS

Bredigite, Poly lactic acid, Porosity gradient, Bone tissue engineering, Scaffolds.

Introduction

The critical segmental bone defect is one of the main problems in orthopedics, seriously affecting the patient's health [1]. Although autogenous bone grafting has long been the gold treatment standard, the number of available bones limits its widespread clinical application [2]. For this purpose, bone tissue engineering was suggested in 1987 to obtain artificial bone substitutes for replacement and regeneration [3]. An ideal bone scaffold should have interconnected porous structure, mechanical support, permeability, and bioactivity [4]. Meanwhile, an interconnected porous structure and gradient can effectively improve cell proliferation and growth as well as the transport of nutrients and oxygen,

thereby promoting tissue regeneration [5,6]. One of the most important challenges in bone tissue engineering is to balance the relationship between the porous structure, the mechanical property, and permeability. The natural human bone is commonly formed of two main zones with a porosity gradient, gradually decreasing from the inner cancellous bone to the outer cortical bone. Cancellous bone, also named trabecular or spongy bone, has a high porosity of 50-90% and a large number of fractal-like bubble structures; while cortical bone possesses a low porosity of 5-10% [7]. An ideal scaffold should have three-dimensionally interconnected porosity with gradient pore sizes to assure a rich blood supply, nutrient delivery, and gas exchange to promote in-growth of bone cells and proper mechanical features [4,5,6]. The mechanical property of the composite scaffolds provide appropriate support for the defect place, stimulates bone regeneration and repair, and provides interconnected pores to support the growth of new bone. The advantage of the different radial porous of scaffolds (1) The porous zone in the middle simulates cancellous bone and offers enough space for nutrient delivery, cell growth and survival (2) The outermost dense zone mimics cortical bone, provides mechanical support for bone tissue regeneration [8]. The bone is a connective tissue consisting of collagen (polymeric phase), mineral (ceramic phase), and water. The mineral phase of human bone is formed of a crystalline form of calcium phosphate ceramic similar to hydroxyapatite ($Ca_{10}(PO_4)_6(OH)_2$). A bioactive ceramic elicits a specific biological response at the interface of the material, which results in the formation of a bond between the tissues and the material while a bioresorbable material gradually degrades over time and is replaced with human natural tissues [9]. Bioceramics can be employed as bone grafts due to their low density, chemical inertness, high wear resistance, excellent tissue adherence, and compositional similarities with natural bone. Their brittleness and weak mechanical strength, however, have limited their use. A solution to this problem could be a polymer-ceramic composite, which incorporates the desirable properties of each of the constituent materials. Significant research has already been devoted to developing polymer-ceramic composites for bone graft applications [10]. Owing to its biocompatibility, biodegradability, and non-toxicity, poly lactic acid (PLA) has been considered a promising polymer for tissue engineering and medical applications [11]. Polylactic acid is a hydrophobic polymer with low surface energy and bioactivity. PLA is synthesized from renewable resources and can be used as packaging in packaging in industry or biomaterials for tissue engineering and medical purposes [12,13]. Calcium silicate-based ceramics have been considered for bone tissue engineering applications due to their superior biological and mechanical properties. Compared to hydroxyapatite (HA), these ceramics showed superior mechanical properties, bioactivity, and biocompatibility, making them suitable bioceramics for biomedical applications [14,15]. Bredigite ($Ca_7MgSi_4O_{16}$) is known as calcium silicate-based bioceramic. The presence of calcium, magnesium, and Si ions in Bre has made it an interesting bioactive material. This ceramic has superior mechanical properties compared to HA [16]. Moreover, the dissolution of Bre in the body simulation solution and the formation of ionic products containing Si and Ca improves the cell proliferation on the surface. In this way, Bre powder accelerates integration with living bone and helps repair bone defects in the human body [17]. This can be achieved by increasing the proliferation and differentiation of osteoblast cells, stimulating collagen production, and improving bone growth [17,18]. In addition, Bre is used as a coating material to overcome the slow osseointegration and poor mechanical support of the host bone tissues as well as reducing the rate of implant loosening [19]. Various methods have been used to make PLA-based composite scaffolds, such as solvent casting and special leaching, gas foaming, electrospinning, melt molding, and freeze drying, which suffer from low controllability of structural features such as porosity and morphology. The use of toxic solvents can limit their application, as well. Today, the use of rapid prototyping methods, especially 3D printing, provides a controllable and precise architecture for tissue engineering scaffolds. Fused Deposition Modeling (FDM) is a simple 3D printing process that creates a computer-aided design (CAD) model layer by layer. The ability to control

layer thickness, porosity, and extrusion temperature are among the advantages of the FDM method [20,21]. In a study on FDM-fabricated PLA/hydroxyapatite (HA) scaffolds, the addition of 50 wt.% HA to the polymer matrix resulted in an increase in void percentage and a decrease in stiffness as well as the amorphous structure of the PLA [22]. In previous studies, it is very common to add bioactive mineral fillers to biopolymers in order to fabricate the composite scaffolds. PLA/bioceramic composite scaffolds are very suitable for bone tissue engineering. In such scaffolds, suitable mineral fillers can reinforce the scaffold, and also play a key role in enhancing the cell adhesion, proliferation and differentiation [23]. The CaO-MgO-SiO_2 based bioceramics improved the adhesion, proliferation, and differentiation of MC3T3-E1 cells due to the release of calcium, magnesium, and silicon ions which can serve as the reinforcement of the polymeric scaffolds [24]. Masoud Arastouei et al. reported that adding Akerminite ($Ca_2MgSi_2O_7$) to PLA led to an increase in the mechanical strength. Moreover, the ionic products released from this bioceramics neutralized the acidic products of PLA degradation. The release of Ca, Mg and Si from Akerminite enhanced the cell behavior of MC3T3-E1 osteoblastic cell line [24]. Marjan Eilbagi et al. developed novel nanostructured composite scaffolds containing Bre powders with various Bre amounts (0, 5, 10, and 15 wt.%) using the space holder method. The addition of Bre powder reduced the average pore and grain sizes, which resulted in the promoted mechanical properties of the scaffolds. The HA/Bre composite scaffolds have shown better bioactivity and biodegradability compared to pure HA. Furthermore, HA/Bre scaffolds significantly promoted cell proliferation and differentiation compared to HA scaffolds [25].
This study reports the fabrication of PLA/Bre composites scaffolds with porosity gradient and different Bre contents via fused deposition modeling (FDM), a commercially available RP technique. In our research, we have characterized these controlled porosity PLA/Bre composites scaffolds in the presence of different contents of Bre on the their physical, mechanical, and biological properties.

Materials and Methods

2.1. Materials

Bredigite powder (particle size = 100-129 nm) was synthesized by sol-gel method according to our previously reported procedures [26], Medical grade Poly Lactic Acid (with the mean Molar weight of 10,000) was purchased from Sigma-Aldrich Company (Sigma - Aldrich: GF45989881).

2.2. Fabrication of the PLA – Bre composite scaffolds using FDM

Briefly, PLA solution with a concentration of 10 wt.% was prepared in chloroform and stirred for 3 h at a speed of 200 rpm until reaching a uniform solution. Then, the Bre suspension was obtained in chloroform. To have a uniform distribution and prevent agglomeration, the Bre solutions were sonicated in an ultrasonic homogenizer (Grant XB6: UK) for 10 min. Then, the proper amount of Bre suspension was gradually added to the polymer solution and mixed for 30 min to achieve the uniform composite solutions, including pure PLA and composites with different loads of Bre particles (0, 10, 20, and 30 wt.%). The solutions were dried at ambient temperature. Composites were crushed and entered into the printer cylinder. The printer (FDM: BioFabX2) is a cylinder and piston system that works by applying air pressure. The crushed composite was entered into the cylinder, and the temperature of the cylinder increased to 195°C, and the material melted. Then, by applying wind pressure and based on the three-dimensional design, PLA-Bre composite scaffolds with 0%, 10%, 20%, and 30% Bre nanoparticles were fabricated for 3D printing of bone tissue scaffold. In this research, a group of scaffolds was made with a radial gradient structure imitating natural human bone with a gradual radial decrease in porosity from spongy bone to cortical bone via 3D printing. Two other groups of scaffolds were made with the pore size of the center (similar to spongy bone) and the pore size of the peripheral

zone (similar to cortical bone) to investigate the effect of the porosity gradient on the mechanical properties and some physical properties of the scaffolds (Fig 1).

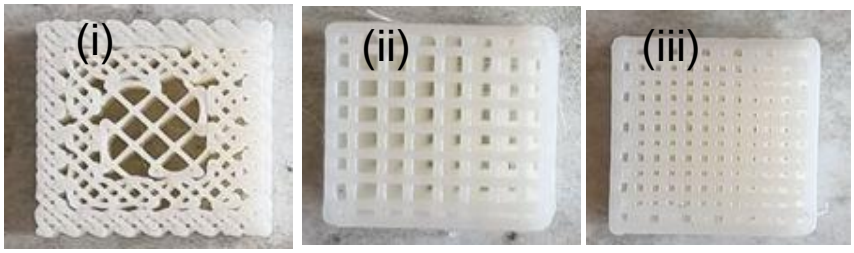

Fig 1.) The representative images of PLA/Bre scaffolds made with (i) porosity gradient, (ii) the pore size of the center (similar to spongy bone) and (iii) the pore size of the peripheral zone (similar to cortical bone).

2.3. Characterization of nanoparticles

A simultaneous thermal analyzer (STA) was used for the detection of possible transformations of the as-dried sol-gel powder. The morphology of the fabricated powders was studied by a field emission scanning electron microscope (FESEM, Philips XL30). The morphology and distribution of elements (Ca, P, Mg, Si) in the synthesized powders and sintered scaffolds were evaluated using a scanning electron microscope (SEM, Phillips XL 30: Eindhoven, Netherlands) coupled with an energy-dispersive spectroscope (EDS, map: EDXA). The mean particle size of Bre was measured by dynamic light scattering (DLS) carried out with a Zetasizer Nano ZS (Horiba SZ -100). To explore the stability of particle suspensions, the zeta potential of the Bre particles was measured with a laser Doppler electrophoresis (LDE) instrument (Nano Series, Malvern Instrument Ltd., UK). To roughly simulate in vivo ionic environments, Bre powders were suspended in physiological saline (0.154 M NaCl solution) at pH 5, 7.4, and 9. The suitability of such in vitro studies was addressed by Bagambisa et al. [27], who found that an aqueous in vitro model yielded complementary results when compared to the in vivo findings because of the ubiquitous presence of water. The zeta potential was measured six times (each measurement being the average of 40 runs), and the mean values and standard deviations were calculated. The instrument automatically calculates electrophoretic mobility (U) and zeta potential according to Smoluchowski's equation [28]:

$$\zeta = U\eta/\varepsilon \quad (1)$$

Where ζ is the zeta potential, U denotes the electrophoretic mobility, η represents the medium viscosity, and ε is the dielectric constant. X-ray diffraction (XRD) analysis was performed for phase analysis of the synthesized powders (Philips X'Pert – MPD System).

2.4. PLA/Bre composite characterization

Rheology is the science of studying the flow and deformation of fluids under the influence of a stress field. One of the most prominent rheological properties of fluids is viscosity, which is a measure of the resistance of fluids to flow or deformation under the influence of an applied stress field. Depending on how viscosity changes in response to applied stresses, fluids are classified into two categories: Newtonian and non-Newtonian. The fluid behavior was determined under different temperatures and stress conditions using a rheometer. Rheometers are used in the calculation of rheological properties in various materials such as non-Newtonian fluids, especially in polymers, thermoplastics, pasty materials, polymer solutions, resins, adhesives, and biopolymers. In this test, the viscosity of PLA-Bre composites was examined with different percentages of Bre (10%, 20%, and 30%) at 100 to 260 ˚C.

The chemical composition of PLA-Bre was explored using X-ray diffraction (XRD, X'Pert Pro X-ray

diffractometer, Phillips, Netherlands) technique carried out with CuKα radiation (λ = 0.154 nm) at a generator voltage of 40 kV.
The chemical composition of the composite PLA-Bre was also confirmed through Fourier transform infrared spectroscopy (FTIR) (Bomem, MB 100) over a range of 600– 4000 cm^{-1} at a resolution of 2 cm^{-1}.

2.5. Mechanical properties of composite scaffolds

To investigate the mechanical behavior of three groups of composite scaffolds, compressive strength, and modulus were estimated using a compression test machine (Hounsfield, H25KS) at room temperature on three specimens (with the dimensions of 10×10×10 mm^3) for each group at a speed of 1 mm/min. Compressive modulus was calculated based on the slope of the initial linear portion of the stress-strain graphs. The compression test was conducted according to the ASTM F2150-19 standard with a cross-head speed of 0.5 mm/min up to 70% strain on the specimens with the dimensions of 10*10*10 mm^3 at the ambient temperature. Compressive modulus was calculated via the slope of the initial linear portion of the stress-strain graphs for scaffolds. This test was repeated 3 times for each sample.

2.5.1. Analysis of finite element simulation software

To simulate the pressure test and analyze the stress on scaffolds with radial gradient, ABAQUS simulation software was employed. The effect of porosity gradient was also investigated on scaffolds mechanical properties. First, the scaffold was designed in 3D design software and entered as a piece of the finite element analysis modeling software. In the next step in the material section, material properties were obtained, including density, elasticity, and plasticity, from a standard sample pressure test, which were then entered into the software. Subsequently, the properties were entered into the software. The boundary conditions of the finite element analysis modeling were set to simulate the uniaxial compression process of the 3D-printed scaffolds.

2.6. Contact angle measurements

The wettability of the composite scaffolds was evaluated by means of dynamic constant angle measurement (VCA optima, AST, Inc.) equipped with a precision camera to capture dynamic images of the droplets.

2.7. In vitro degradation behaviors

The in vitro degradation rate of the composite scaffolds was investigated by measuring their weight loss during soaking in PBS using the method suggested by Huang et al. [29]. In this study, the samples were immersed in phosphate buffered saline (PBS) with azide sodium 0.1% (w/v) pH = 7.4 and kept in an incubator for up to 28 days at a uniform temperature of 37 °C. Firstly, samples of composite scaffolds with a rectangular cross-section (1 × 1 cm^2) were weighed on a scale with accuracy up to 0.0001 g and immersed in 5 ml of PBS solution containing 0.1% (w/v) sodium azide under constant stirring at 37 °C in the incubator. At specific intervals, the pH value of the PBS solution was measured by pH meter and exchanged with fresh PBS containing 0.1% (w/v) sodium azide to ensure a constant pH =7.4. After each degradation period (7, 14, 21, 28 days), the specimens were washed with deionized water and dried in a vacuum oven at room temperature overnight. Ultimately, the weight loss after the degradation test was calculated using the following equation (2):

$$Weight\ loss = [\ (M_0 - M_d) / M_0] \times 100 \quad (2)$$

Here, M_0 and M_d are the dried weights of PLA/Bre scaffolds before and after the degradation period measured by analytical balance, respectively.

2.8. In vitro bioactivity assays

In vitro bioactivity of composite scaffolds was studied by soaking specimens in a Simulated Body Fluid (SBF) solution. The SBF was prepared as reported by Kokubo et al. [30], and the scaffolds were immersed in it at 37 *℃* for specified periods up to 28 days. Apatite formation on the surface of the scaffolds was investigated by SEM equipped with EDS, and Fourier transform infrared (FTIR) tests were also used to evaluate the formation of apatite on the surface of both the pure PLA and composite scaffolds. SBF solutions were collected at regular intervals to measure the ion concentrations of Ca, Mg, and P by inductively coupled plasma atomic emission spectroscopy (ICP) (AES; Varian, USA). In addition, the pH values of the solution during scaffold soaking were investigated.

2.9. Cell culture assay

Biocompatibility of the coatings (n = 3) was investigated using an MG63 cell line from the Royan Institute of Iran. The MG63 cells were cultured in complete culture medium (DMEM-low, containing 10% (v/v) fetal bovine serum (FBS, Bioidea, Iran) and 1 (v/v) % streptomycin/penicillin (Bioidea, Iran)) at 37 °C under 5% CO_2. The culture medium was refreshed every 3 days. Before cell culture, the specimens were sterilized for 60 min in 70% ethanol and 6 h under UV light. As a result, the samples were immersed in the complete culture medium for a day just before cell seeding. Consequently, 104 cells were seeded on the specimens as well as tissue culture plate (TCP, control), and cell-seeded samples were shown at 37 °C under 5% CO_2 condition for 7 days, and the medium was refreshed every 3 days.

2.9.1. Cell viability assay

The relative viability of cells was investigated by 3-(4,5-dimethylthiazol-2-yl)-2,5-diphenyltetrazolium bromide (MTT), according to the manufacturer's protocol (Sigma-Aldrich). At the specific time points, after removing the culture medium, 500 µl of MTT solution (0.5 mg/ml in a phosphate buffer solution (PBS)) was spilled into each well. After 4 h incubation at 37 °C under 5% CO_2, the formazan purple crystals were dissolved in dindimethyl sulfoxide (DMSO solution, Sigma). The purple solution was then placed in 96-well plates, and their optical density (OD) was measured at the wavelength of 490 nm using a microplate reader (Biotech) against DMSO (blank). Ultimately, the relative cell viability was expressed as follows [30]:

$$\textit{Relative Cell Viability (\%)} = [\,(A_{sample} - A_{blank}) / (Ac_{ontrol} - A_{blank})\,] \times 100 \quad (3)$$

A_{sample}, A_b and A_c are the absorbance of the sample, blank (DMSO) and control (TCP), respectively.

2.9.2. Cell morphology study

The morphology of the cells seeded on the samples was evaluated by the SEM technique. The cells were fixed with 2.5% glutaraldehyde solution (Sigma) for 3 h, after 7 days of cell culture. Then, the cell-seeded samples were washed two times with PBS and dehydrated in the graded concentrations of ethanol (30, 70, 90, 96, and 100 (v/v) %) for 10 min, respectively. After complete drying at room temperature, the specimens were imaged using SEM.

2.10. ALP activity assay

ALP expression was evaluated on the 3rd and 7th days of cell culture through ALP activity assay. The ALP activity MG-63 in the scaffolds was assessed through the dephosphorylation of para-nitrophenylphosphate (pNPP) and its conversion to para-nitrophenol (pNP). In this assay, the cultured cells were rinsed with PBS and dissociated from the surface of the samples through trypsinization. Then, they were soaked in a lysis buffer (25.0 mM HCL-Tris containing 1% Triton X-100, pH = 7.5) and centrifuged for 10 min at 12,000 rpm. The prepared samples (20 µL) were added to 1 mL of the kit

solution in a 96-well plate, and read by a microplate reader device at the wavelength of 405 nm [31].

2.11. Alizarin red assay

Alizarin red assessment was run on the samples to assay calcium deposits on the 3rd and 7th days of cell culture. The culture medium was removed and replaced with 300 µL of 10 % formaldehyde solution. The prepared samples were washed with PBS after 20 min, and 500 µL of 40 mM alizarin red solution was added to the cell-contained samples. Samples were transferred to a shaker plate for 20 min. Next, the samples were washed several times with distilled water to eliminate excess dyes. The absorbed stains were observed by a stereoscope. Then, 400 µL of 10 % acetic acid was added to each sample and kept at room temperature for 30 min in tubes. The samples were placed in vortex for 30 min at room temperature. They were heated at 80°C for 10 min. The tubes of samples were incubated on ice for 5 min, and the prepared slurry was centrifuged for 15 min. The supernatant was transferred to a new tube containing 200 µL of 10 % ammonium hydroxide, and ultimately, the absorbance was read at 405 nm by an ELISA reader [32].

2.12. Statistical analysis

Statistical analyses were performed using Tukey's Post hoc test by Graph Pad Prism Software (V.6). The values were reported as the mean (n = 3) and expressed as mean±SD. One-way ANOVA was used to determine the statistical differences ($P<0.05$).

3. Results and discussion

3.1. Characterization of Bre powder

STA analysis was carried out to investigate the phase changes during the heat treatment of as-dried bredigite powder at 120 ˚C for 48 h (Fig. 2a). The weight loss occurs within three stages, leading to a total weight loss of 16%. The first weight loss (7 %) occurred below 350°C, which might be due to the loss of adsorbed water molecule and remaining solvent (ethanol) [33,34,35]. Weight losses (9%) in the temperature range of 500-600 ˚C can be attributed to the dehydration of calcium nitrate tetrahydrate, decomposition of organic matter, and elimination of alkoxyl groups and burning of carbon and elimination of residual nitrates introduced by metal nitrate during the preparation of the sol [33,36,37]. The third stage of weight loss, observed in the temperature range of 600- 1200 °C, can be assigned to the crystallization of bredigite powder as confirmed by the XRD (Fig.2c) [33,36,38].

The FESEM image of Bre powder in Fig. 2b revealed the nano-scale nature of the Bre particles. This micrograph shows the formation of agglomerated nanometer (100-130 nm) particles (Fig. 2b). The particle size distribution and the intensity of the bredigite dispersions were also measured by DLS (Fig. 2d). The cumulants analysis of the correlation function indicates the average size of Bre nanoparticles of 100 ± 26 nm.

Fig. 2c shows the X-ray diffraction (XRD) pattern of the dried powder heat-treated at different temperatures (1150 and 1250 °C for 2 h at a rate of 10 °C/min). The XRD patterns of the Bre powder showed its successful synthesis with sol- gel method with high purity. A similar XRD pattern was reported elsewhere [34]. Zeta potential for Bre particles is negative (-17/5 mv). According to the reports, negative zeta potential has an important biological effect in the body environment [28], and low zeta potential can improve cell proliferation and adhesion [39]. Some studies showed that in materials with negative surface energy (negative zeta potential), the possibility of proliferation and adhesion of bone-forming cells is higher than in surfaces without charge or surfaces with positive charge [40]. Zeta potential for Bre particle is negative. According to the reports, negative zeta potential has an important biological effect in the body environment [28] and low zeta potential has improved cell proliferation and adhesion [41,42]. Some studies showed that in materials with negative surface energy (negative

ISSN 1019-6609
eISSN 1853-4961

zeta potential), the possibility of proliferation and adhesion of bone-forming cells is higher than surfaces without charge or surfaces with positive charge [42].

Table 1. Measuring the surface charge of particles (zeta potential).

Powder sample	**)mv(Zeta potential**
Bredigite	-17.2

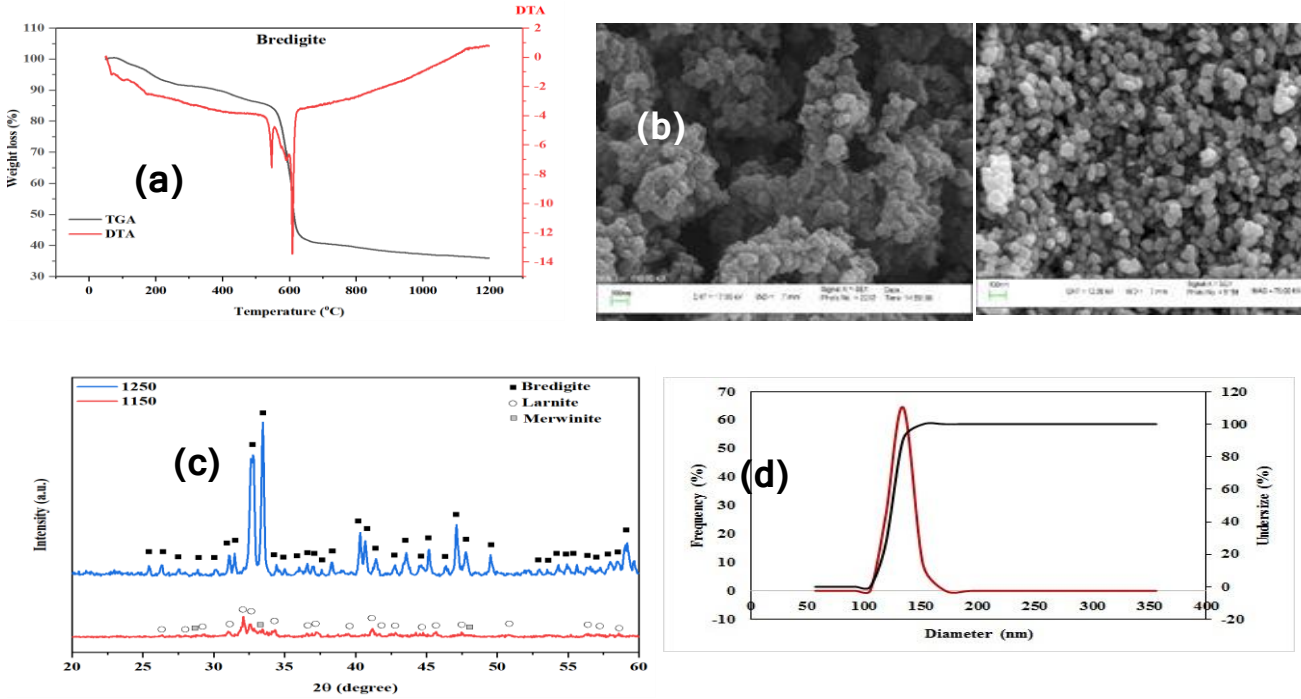

Fig 2. Characterization of Br nanopower: a) TG/DTA curves of dried gel bredigite nanopowders dried at 120 ◦C for 48 h. b) FESEM image of bredigite powder in 1150, 1250 ◦C c) XRD patterns Bredigite powder at 1150, 1250 ˚C d) DLS analysis.

3.2. Characterization of the PLA / Bre composite

This study comprehensively investigates the rheological properties of polylactide (PLA)-based composites reinforced with Bre particles. The primary objective is to evaluate the influence of Bre particle content (10%, 20%, and 30% by weight) and temperature (ranging from 100 to 250°C) on the flow and viscoelastic behavior of these composites (Fig. 3). The findings provide crucial insights into the processability and potential applications of these materials. As clearly illustrated in Figure 3, the dynamic viscosity for all three PLA/Bre composite samples consistently decreases significantly with increasing temperature. This inverse relationship between viscosity and temperature is a universally expected rheological behavior for thermoplastic polymers and their composites [43]. Elevated thermal energy increases the mobility of polymer chains, thereby reducing internal resistance to flow [44]. At lower temperatures (e.g., 100°C in Figure 3), the initial viscosity of the samples followed a specific order: PLA-20% Bre > PLA-30% Bre > PLA-10% Bre. The observation that the initial viscosity of the PLA-20% Bre sample was higher than that of the PLA-30% Bre sample is noteworthy. This phenomenon could potentially be attributed to a more optimal and homogeneous distribution of ceramic particles within the polymer matrix, coupled with enhanced interphase interactions at the 20% concentration, leading

ISSN 1019-6609
eISSN 1853-4961

to a more effective increase in flow resistance [45]. However, as the temperature increased towards 250°C, the viscosity differences between the samples diminished, and the curves converged to similar low values (approximately 0.07-0.08 Pa·s). This convergence at high temperatures suggests that under these conditions, the material's flow behavior is predominantly influenced by the mobility of the polymer chains, with the role of reinforcing particles becoming less significant compared to lower temperatures [46]. Both the storage modulus (G'), which represents the stored elastic energy and the material's elastic character, and the loss modulus (G''), which signifies dissipated energy (viscous loss) and the material's viscous character, were observed to increase with higher filler concentrations. This increase indicates mechanical reinforcement and enhanced stiffness of the composite upon the addition of rigid Bredigite particles [47]. A significant inflection point in the G' and G'' curves was identified within the temperature range of 168-174°C. This inflection point suggests a transition in the flow behavior towards shear-thinning under the influence of increasing temperature [48]. A downward trend in both G' and G'' was consistently observed for all three samples up to the maximum testing temperature of 250°C. Up to 195°C, the loss modulus (G'') in all three samples decreased by a maximum of 5%, indicating a relatively good thermal stability of the composites within this temperature range. This minor decrease can be attributed to various factors, including the release of entrapped air bubbles, a slight reduction in the sample's elasticity, or changes in residual transverse connections within the polymer network [49]. However, at temperatures exceeding 195°C, a sharp and instantaneous decrease in both G' and G'' was observed. This rapid decline, indicative of a significant reduction in the material's rigidity and hardness, is most likely influenced by the onset of structural disintegration of the polymer in response to the elevated temperatures [50]. While an increase in ceramic particle content from 20% to 30% would typically lead to an increase in viscosity and moduli (G' and G''), the excessive increase in additive percentage and consequently, the increased contact surface between ceramic particles, can lead to particle agglomeration [51]. This agglomeration, rather than promoting a more uniform distribution, results in the formation of larger structures and entangled networks of particles within the polymer matrix. Such agglomeration significantly increases the resistance to fluid flow, thus leading to an elevated viscosity [52]. This distinct effect of agglomeration contrasts with the benefits of a more uniform distribution observed at 20% Bre. Another notable observation is that at high temperatures, ceramic particles can sometimes act as lubricants. They achieve this by reducing friction between polymer molecules and facilitating their movement, which may explain the greater decrease in viscosity observed at high temperatures in the 20% and 30% Bredigite samples compared to the 10% Bredigite sample [53].

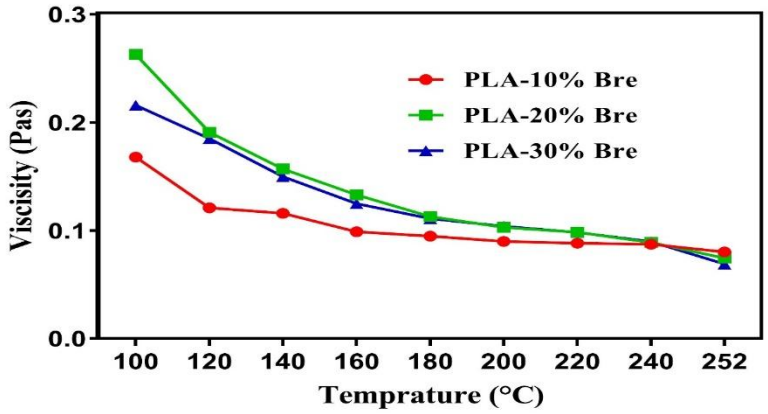

Fig 3. Rheology characteristics of Bre / PLA composite.

ISSN 1019-6609
eISSN 1853-4961

The presence of Bre particle within the PLA matrix was also investigated by XRD and FTIR studies (Fig.4). The XRD pattern of the PLA scaffold (Fig. 4a) consisted of PLA characteristic peaks at 2θ = 20˚. The presence of the characteristic peaks of Bre in the XRD patterns of the PLA-Bre scaffolds, specifically at higher Bre content (20 and 30 wt. %), confirmed the presence of Bre in the composite scaffolds.

The ATR-FTIR spectra of the composite scaffolds are shown in Fig. 4b. The pure PLA scaffold exhibits 8 critical inferred bonds. The absorption peak at 1748 cm^{-1} is due to CO = characteristic group, while two peaks at 1083 and 1181 cm^{-1} are related to C–O stretching [48]. Moreover, the peaks appearing at 2920 and 2996 cm^{-1} demonstrate asymmetric and symmetric stretching of CH3 [54]. The peaks at 753 and 856 cm^{-1} indicate C-H and C-C vibrational bonds, respectively. [55]. The band at 1451 cm^{-1} also corresponds to stretching vibrations [54]. Followed by combining the Bre in PLA scaffold, several bands appear. The peaks in the range of 1100-1000 cm, 960 cm, and 873 cm^{-1} are related to SiO_4 stretching. However, the peak at 616 cm^{-1} indicates SiO_4 bending. The band at 530 cm^{-1} can be ascribed to Ca-O stretching [54]. Thus, the whole characteristic bands of PLA and Bre suggests the physical interactions between PLA and Bre.

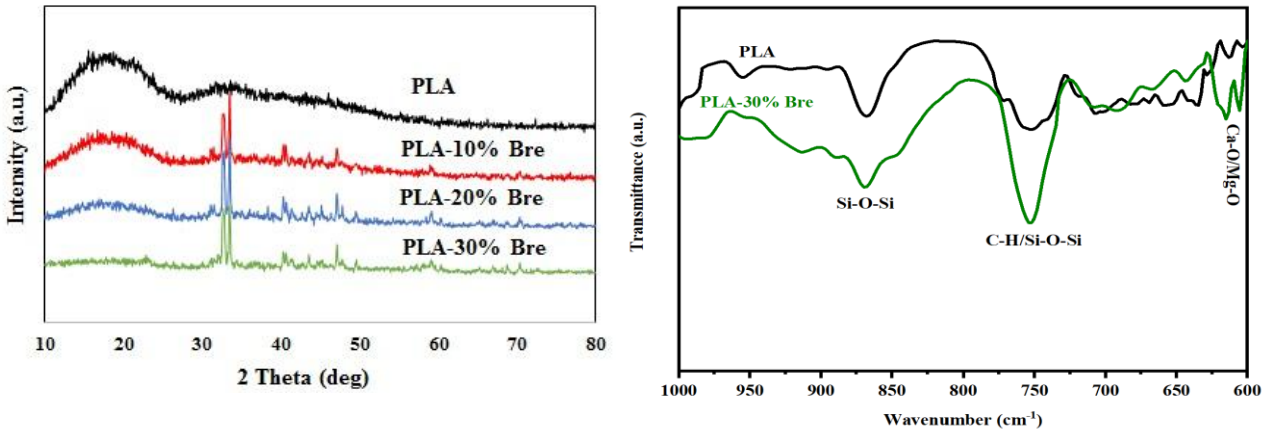

Fig. 4. a) XRD patterns and b) ATR-FTIR spectra of composite scaffolds containing 0%, 10 %, 20 % and 30 % of Bre.

3.3. The structural properties of PLA/Bre scaffold

Porous scaffolds are used to enhance cell proliferation and tissue regeneration. In the current study, nanocomposite scaffolds were fabricated by the incorporation of Bre into PLA scaffolds via FDM for the treatment of bone defects (Figs. 5b, c). Fig. 5a shows image of PLA, PLA/Bre 10 wt.%, PLA/Bre 20 wt.%, and PLA/Bre 30 wt.%. As seen, all scaffolds have a gradient of porosity that simulates human bone with open and interconnected pores. The porous zone in the center simulates cancellous bone and provides enough space for oxygen and nutrient delivery, cell survival, and growth and the outermost dense zone mimics cortical bone, providing mechanical support for tissue repair and regeneration, while preventing fibrous tissue from growing and tissue regeneration [8]. The images of the printed scaffolds showed that, all PLA, PLA/Bre 10 wt.%, and PLA/Bre 20 wt.% were crack-free, but the PLA/Bre 30 wt.% scaffold contained cracks in some areas due to lower processability of PLA/Bre 30 wt.% in comparison to other scaffolds. According to Fig.5b, the average pore size of the scaffolds decreased with increasing the Bre particle content. Moreover, SEM images of the PLA/Bre scaffolds showed coarser and more uneven surfaces.

The EDX spectrum of the PLA / 20wt.% Bre scaffold (Fig.5c) also confirmed the presence of Ca in the nanocomposite scaffolds and the presence of Bre particles in PLA scaffolds. The EDS-mapping analysis of the PLA/Bre scaffold (Fig.5d) also showed that Bre particles were dispersed in the PLA matrix,

ISSN 1019-6609
eISSN 1853-4961

without any agglomeration up to 20 wt. % Bre. However, the agglomeration of nanoparticle was detected when the Bre content in PLA matrix was elevated to 30 wt. %.

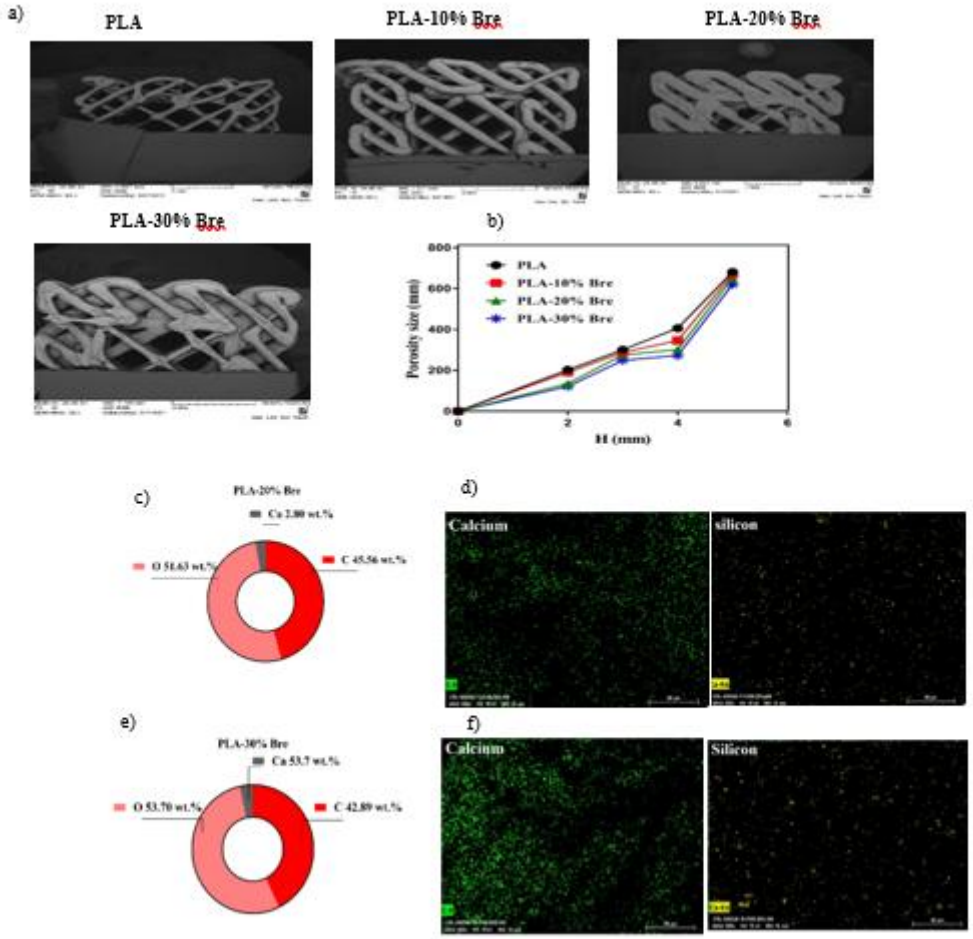

Fig. 5. a) SEM image of surface morphology of the PLA, PLA- Bre scaffolds. b) Average pore size of the PLA and PLA-Bre scaffolds. c) EDX spectrum of PLA- 20 Bre Scaffolds. d) EDS mapping analysis of PLA- 20 Bre scaffold. e) EDX spectrum for PLA- 30 Bre Scaffolds. f) EDS mapping analysis of the PLA-30 Bre scaffold.

3.4. Mechanical properties

In other words, the mechanical properties decreased in the scaffold with the pore size of the center (similar to spongy bone) and scaffolds with the pore size of the peripheral zone (similar to cortical bone) compared to scaffolds with a porosity gradient due to the increased porosity volume. The mechanical properties of scaffolds with large pore sizes are reduced due to the increase in the volume of void spaces as larger voids reduced the resistance to compression and tension [56]. In two groups of scaffolds without porosity gradient, this trend can be attributed to the particular pore structure and high porosity. Ceramic-incorporated composites must contend with problems including, but not limited to, agglomeration of ceramic particles, inadequate dispersion of the ceramic phase, and poor attachment at the ceramic-polymer interface [56,57]. These problems can cancel the advantages of a composite structure and lead to a significant reduction in mechanical properties. At Bre powder contents above 30 wt.%, the relatively weak interfacial PLA/Bre interactions and agglomeration of the Bre powder during the fabrication of scaffolds could lead to the reduction of mechanical properties. Additionally,

ISSN 1019-6609
eISSN 1853-4961

the presence of the Bre in the polymeric matrix also had a significant effect on reducing porosity and pore size of the scaffolds and also Bre particles with a better elastic modulus and compressive strength (compared with pure PLA) can serve as a stiff filler and enhance the stiffness of the PLA/Bre scaffolds. Arastouei et al. [58] fabricated PLA / Akermanite scaffold by fused filament fabrication (FFF) technology and reported an increment in the compressive strength with increasing the Akermanite content (27±2 MPa to 45±3 MPa). Shiota et al. [59] showed that the compressive strength of HA/β-TCP decreased with increasing β-TCP content. Based on previous data, reduction of β-TCP phase with increasing Bre content could also improve the mechanical properties of composite scaffolds. β-TCP composite scaffolds containing different Bre contents (25, 35, 45 wt.%) were fabricated by the space holder method and with a homogeneous microstructure and interconnected pores. The compressive strength of the βTCP/25 Bre scaffold was approximately twice of the pure β-TCP scaffold and similar to the trabecular bone. However, adding more Bre reduced the compressive strength due to the agglomeration of Bre phase at the grain boundaries [60]. Here, we expanded a bone-mimicking radial-gradient scaffold to provide appropriate support for the defect site, stimulates bone regeneration and repair, and prepares interconnected pores to support the growth of new bone.

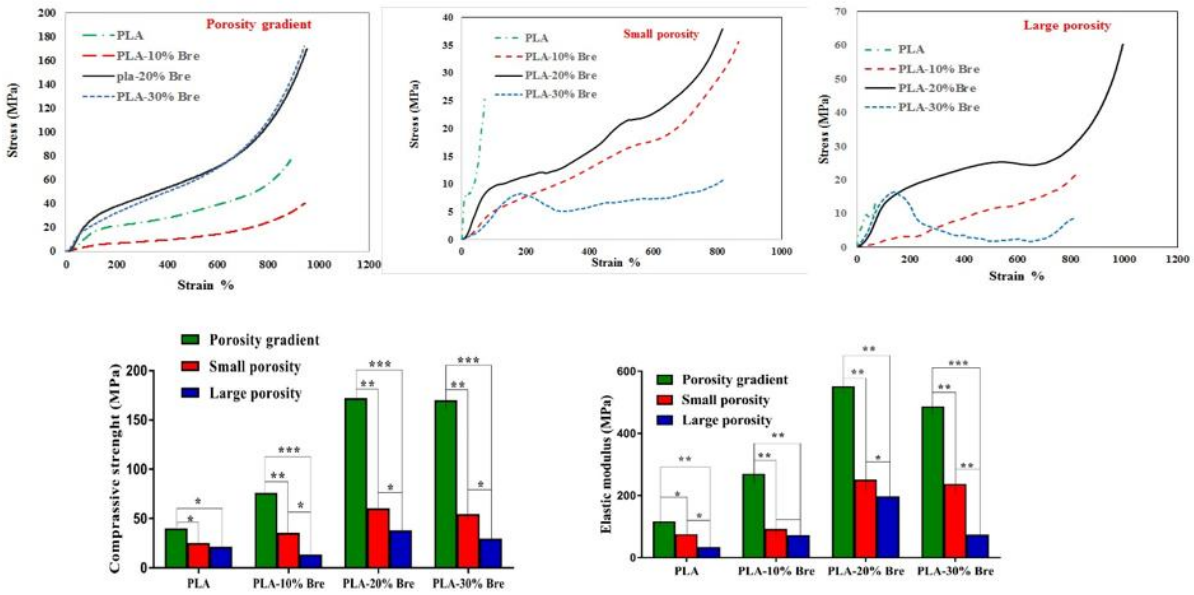

Fig. 6. a) Stress-Strain diagram of PLA scaffold with different percentages of Bre b) compressive strength and c) elastic modulus of PLA and PLA/Bre scaffolds containing various Bre contents.

3.4.1. Finite element simulation

Figure 7 presents the results of the finite element simulation conducted in the Abaqus environment. The boundary conditions for the modeling of the PLA-Bre composite scaffolds were set to simulate the uniaxial compression process of the 3D-printed scaffolds. The comparison of experimental and simulation results demonstrated good agreement between the predicted model and the experimental outcomes, indicating high accuracy for this gradient model. The PLA-Bre scaffold features a bone-mimicking radial-gradient with a fractal-like structure, designed such that its properties gradually increase along the radial direction. This design effectively meets the requirements for the mechanical support performance of natural bone, transitioning from cancellous bone to cortical bone. Although the simulated compressive modulus was consistently higher than the experimental modulus, both

ISSN 1019-6609
eISSN 1853-4961

simulation and experimental methods showed similar trends in mechanical properties, with an increase observed along the radial direction. The mechanical characteristics of the PLA-Bre scaffold are designed to provide appropriate support for the defect site, thereby stimulating bone regeneration and repair, and preparing interconnected pores that facilitate the growth of new bone.

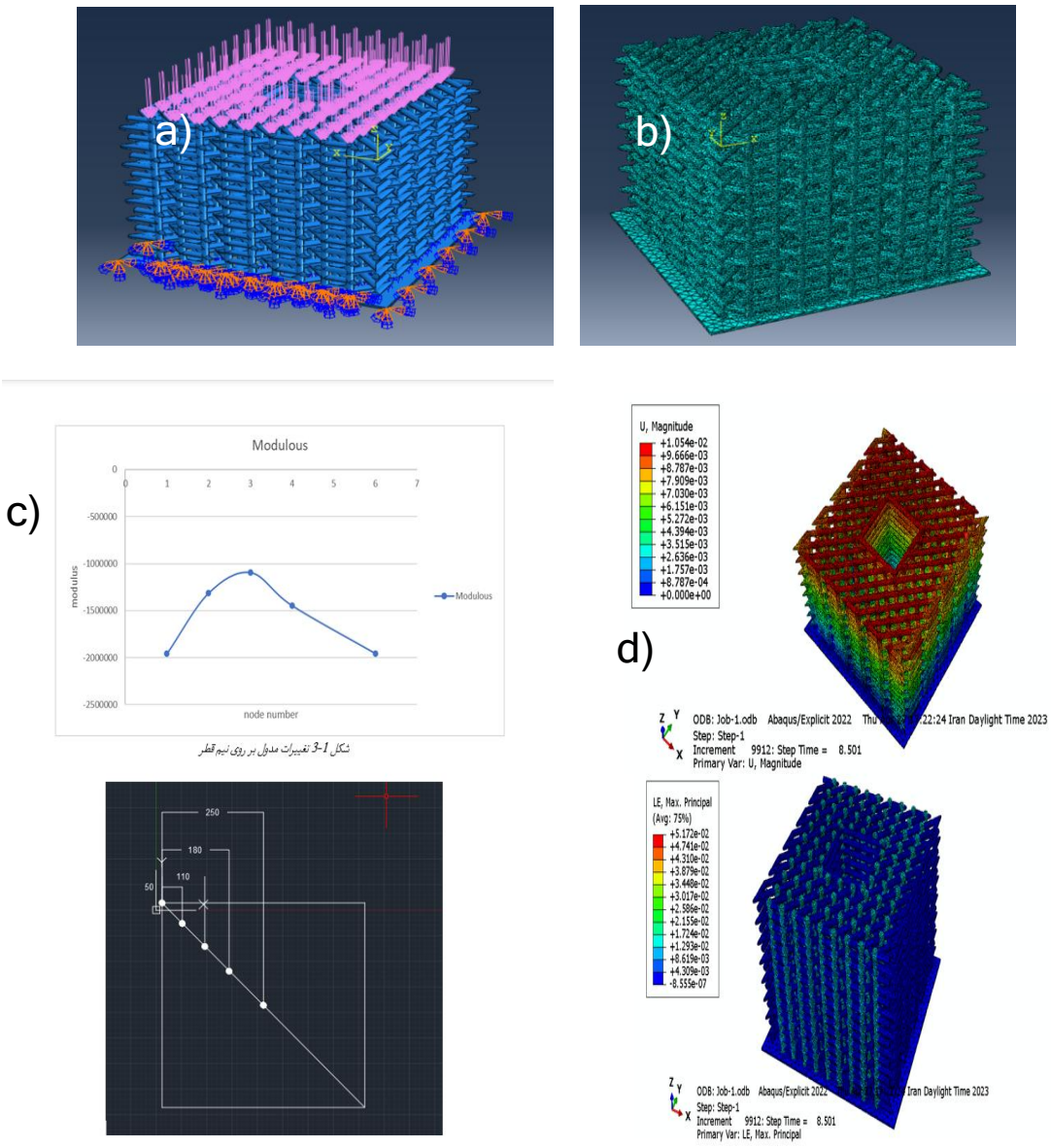

شکل 1-3 تغییرات مدول بر روی نیم‌قطر

Figure 7 a) A view of the definition of constraint and load on the model b) Meshing in Abaqus software on the 3D model c) Radial elastic modulus measurement points and modulus changes on the radius of the model d) Display of displacement in the Abaqus software and display the strain and stress in the Abaqus software.

3.5. Wettability of PLA/Bre scaffolds

Figure 8 illustrates the water contact angles of the scaffold surfaces. As depicted, the water contact angles for PLA/Bre composite scaffolds initially decreased significantly with increasing Bre content. Specifically, the contact angle reduced from approximately 88° for pure PLA to about 70° for PLA-

ISSN 1019-6609
eISSN 1853-4961

20%wt. Bre. This reduction in contact angle directly indicates an improvement in the hydrophilicity of the composite scaffolds, which is generally desirable for biological applications. However, it was observed that the water contact angle for the PLA/30%wt. Bre scaffold (approximately 77°) was higher than that of the PLA/20%wt. Bre scaffold. This finding suggests that while the incorporation of Bre initially enhances wettability, there appears to be an optimal Bre concentration (e.g., 20%wt.) beyond which further increase in Bre content leads to a slight reduction in hydrophilicity. This behavior could be attributed to changes in surface morphology, such as increased surface roughness at higher filler concentrations leading to air entrapment, or potential agglomeration of Bre particles, which may reduce the effective hydrophilic surface area [61].

The observed variations in contact angle highlight the intricate relationship between surface roughness, porosity, pore size, and scaffold hydrophilicity. Specifically, the higher porosity of the PLA/20%wt. Bre scaffold (compared with PLA/30%wt. Bre). likely resulted in a reduced contact angle due to the enhanced capillary absorption of water droplets by the composite [62]. Conversely, in instances where surface roughness is sufficiently high, the peaks of the roughness can entrap fluid, leading to metastable states of the water drop. This phenomenon can result in an increase in the contact angle and a subsequent reduction in hydrophilicity [63,64] Overall, a higher specific surface area, often associated with increased porosity and improved wettability, generally results in scaffolds with a more hydrophilic character. This enhanced wettability is crucial as it makes the scaffolds more suitable for bone regeneration and facilitates better cell adhesion and nutrient exchange.

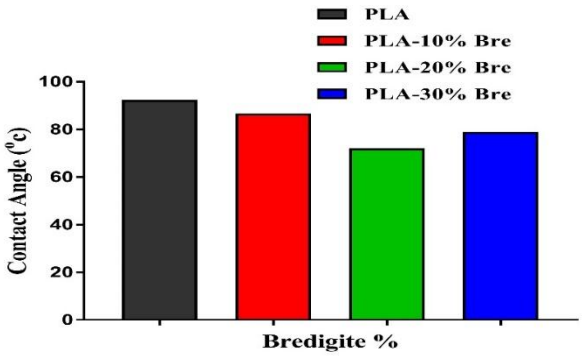

Fig.8. Effect of the weight percent of Bre on the composite scaffolds of wettability.

3.6. In vitro degradation behaviors

Figure 9a shows the weight loss of pure PLA and composite scaffolds soaked in PBS. Weight loss of pure PLA occurs very slowly, without noticeable weight change throughout the degradation period. A slight increase in weight for pure PLA is primarily due to water absorption by the polymer. In contrast to the pure PLA scaffold, weight loss in the composites was significantly higher and increased progressively throughout the incubation period in proportion to the Bre powder content. The increased weight loss of the composite scaffolds can be mainly attributed to the degradation of Bre powder and the release of ions in the solution, a phenomenon facilitated by the hydrophilicity of Bre.

Figure 9b depicts the pH changes of the PBS solution as a function of immersion time. As observed, the pH of the incubation medium slightly decreased from 7.4 in the presence of the pure PLA scaffold, owing to the acidic products of PLA degradation. Conversely, the pH values of solutions containing composite scaffolds with high amounts of Bre powder (30 wt.% Bre) increased during the first three days of incubation. This increase is attributed to the release of alkaline ions (such as Ca and Mg) from Bre particles, which locally compensate for the acidification of the medium caused by acidic products of the polymer degradation. This buffering role of Bre is another significant advantage in the composite

ISSN 1019-6609
eISSN 1853-4961

scaffolds, as it helps in mitigating inflammatory responses that may arise from the acidic decomposition of the polymers. Similar buffering effects have also been reported in forsterite bioceramics [65].

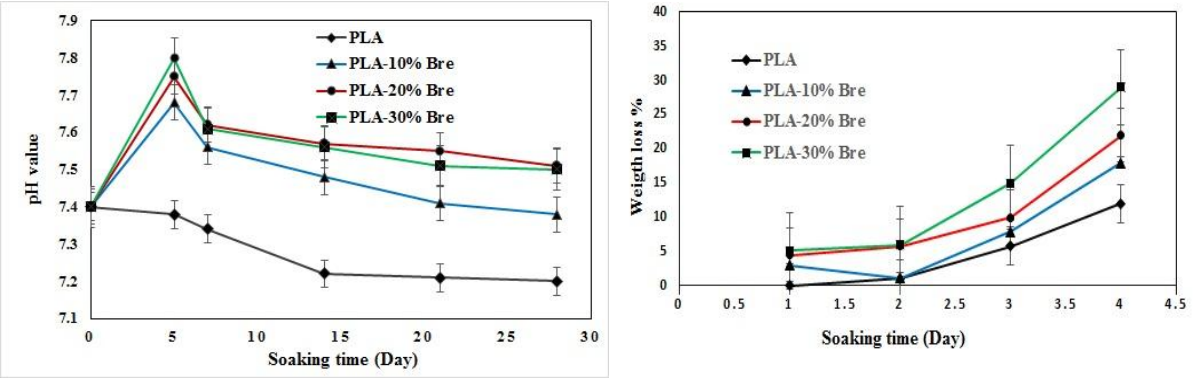

Fig.9. a) weight loss of PLA and PLA / Bre scaffolds following soaking in PBS. b) The changes of the pH value of the PBS solution during the soaking of the PLA and PLA / Bre scaffolds.

3.7. In vitro bioactivity of composite scaffolds

Biomaterials that are grafted to living bone must form an apatite layer after being implanted in the body. In vitro bioactivity of the composite scaffolds was evaluated by soaking the samples in SBF and investigating the formation of apatite on their surfaces. Fig. 10 represents SEM micrographs and EDS results of the pure PLA and PLA-20%wt. Bre composite scaffolds after soaking in SBF for a period of 28 days. No signs of Ca/P formation was observed on the surface of pure PLA scaffold (Fig. 10a). In the presence of 20 wt.% Bre powder (Fig. 10b), spherical particles with needle like crystallites were formed on the surfaces and the pore walls of the composite scaffolds. Moreover, the number and size of the Ca/p particles rose on the surface of the PLA-Ak 30 wt.% scaffold after 28 days of immersion in the SBF [42]. By increasing the Bre content up to 30wt.%, the surface of the scaffolds was covered with apatite crystals and the surface morphology of the composite scaffold immersed in SBF changed, reducing the Ca: P ratio. Previous studies on the Si-containing bioceramics such as bioglass indicated higher bioactivity than pure HA [47]. Kokubo et al. [48] reported that silica plays an important role in the improved nucleation and growth of bone-like apatite layer on the bioactive composite scaffolds. According to the above results, the composite scaffolds of PLA and Bre powder can induce the formation of a Ca/P layer on their surfaces in SBF which is essential for bone tissue engineering applications.

The surface of PLA and PLA/20% wt. Bre after soaking in SBF for 28 day was characterized by FTIR spectroscopy to analyze absorption bands of different functional groups and confirm the formation of apatite (Fig. 10c). The peaks appearing at 963, 1081, and 1144 cm^{-1} in PLA are related to the stretching vibration of P=O bonds and the asymmetric and symmetric stretching vibrations of P-O bonds in the phosphate structure, respectively, due to deposition of apatite on the surface of the sample [49,50]. The intensity of the characteristic peaks in the sample containing Bre is higher than the neat PLA, indicating the formation of more apatite in the sample containing Bre. The peaks at 1182, 1079, and 1042 cm^{-1} are related to the stretching vibration of P=O bonds and the asymmetric and symmetric stretching vibrations of P-O bonds due to apatite precipitation on the surface Bre-containing sample [48,49]. The peaks located at 1872 and 1622cm^{-1} are related to the bending modes of phosphate while the band at 1755 cm^{-1} corresponds to carbonate functional group. The stretching vibration of Ca-O and Mg-O bonds in the Bre structure can be detected at 1622cm^{-1} which indicated the presence of Bre particle in the composite scaffolds [50,51,52].

ISSN 1019-6609
eISSN 1853-4961

As can be seen, the pH values of the pure PLA scaffold did not significantly change after the first 7 days of soaking, after that, it started to become slowly acidic. In the composite scaffolds, the pH of SBF solution increased in the first 7 days, followed by a slow decreasing trend till the end of the soaking period. According to the obtained results, the increasing rate of pH and its value depend on the Bre powder content. In the presence of Bre powder up to 20 wt.%, the pH values did not clearly change, and at the end of these 28 days periods, the pH values were in about the initial values. Increasing the Bre powder loadings up to 30 wt.% leads to more drastic pH changes. Interchange of Ca^{2+} and Mg^{2+} released from Bre with H^+ or H_3O^+ from SBF solution and formation of silanol bond (Si–OH) in the initial soaking times enhanced OH^- concentration and pH of the solution, giving rise to apatite nucleation. Following the migration of calcium, phosphate and hydroxyl ions to the surface of scaffolds and nucleation of bone-like apatite, pH of solution slowly reduced, demonstrating the consumption of hydroxyl ions during the formation of apatite layer on the scaffolds contain Bre [54].

Fig. 10d shows Ca and P ions concentrations, based on ICP test, in the SBF used for the immersion of PLA/20 wt.% Bre scaffolds. In the initial stage of soaking (first 3 days), phosphorus and calcium ions were consumed from the SBF solutions toward the surfaces of the scaffolds. It shows a decrease of Ca and the P ions concentration for the composite scaffolds at the end of the 4-week soaking. The in vitro bioactivity test suggests the important role of Bre powder in the nucleation and growth of apatite in SBF. The suggested mechanism of bioactivity of Bre powder in the SBF was explained in previous studies [54].

Results also show that the low wettability of PLA reduce the SBF interaction with the Bre powder in samples with low Bre powder content (≤30 wt.%). Moreover, the higher content of Bre powder in SBF may cause contact and reaction of Bre powder with SBF, leading to the mineralization of apatite.

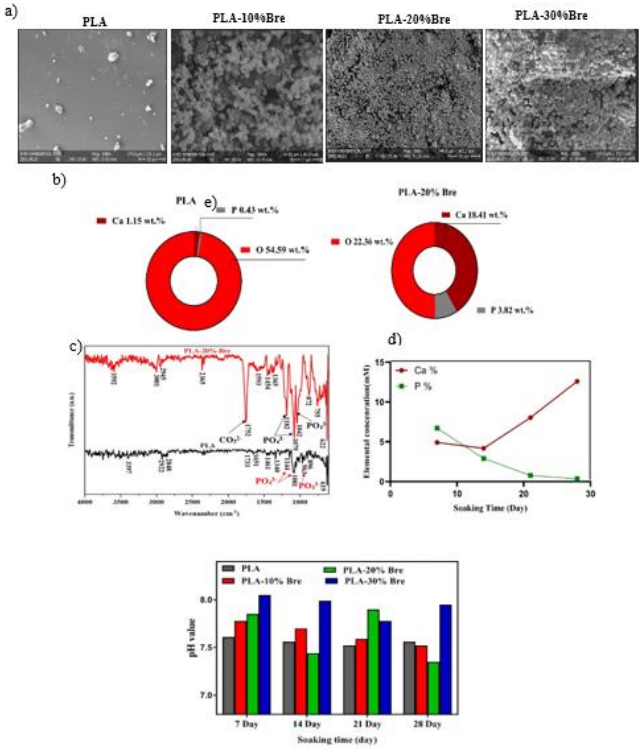

Fig10. a) SEM morphology of the PLA and PLA / Bre scaffolds, after 28 days of incubation in SBF. b) EDX analysis of the PLA and PLA/20% Bre scaffolds after 28 days of incubation in SBF. c) FT-IR spectra of PLA samples without and containing 20 wt% of Bre after immersion in SBF solution. d) The concentrations of Ca and P ions of the SBF solution during the soaking of PLA and PLA/Bre scaffolds e) pH changes of the SBF solution during the soaking of the PLA and PLA/Bre scaffolds.

ISSN 1019-6609
eISSN 1853-4961

3.8. Cytotoxicity assay

Fig. 11 shows the results of the MTT assay of composite and pure PLA scaffolds after 7 days of cell culturing. The OD values serve as an indicator of the relative number of cells. The results demonstrate the much faster cell growth in the composite samples compared to the control one, suggesting non-cytotoxicity of the PLA-Bre composite. Results indicated lower cell proliferation onto the pure PLA scaffold with a significant difference ($p < 0.05$). The hydrophobicity of the PLA sample reduced the cell proliferation capacity. According to the results, cell proliferation on composite scaffolds significantly increased during 3-day culture period ($p<0.001$ or $p<0.05$), which is consistent with previous studies [69]. Although cells exhibited highest proliferation on PLA/20 wt.% Bre, no obvious difference was observed between composite scaffolds with different Bre content ($p>0.05$). It is reported that Bre have more profound effect on cell behavior and viability in comparison with β-tricalcium phosphate (β-TCP) [70]. In another study, the presence of akermanite improved the survival of bone marrow mesenchymal stem cells (MSCs). Moreover, the non-toxicity of CaO-MgO-SiO_2-based bioceramics and their constituents was confirmed in the literatures [73,74]. The release of Si and Ca ions from the CaO-MgO-SiO_2-based bioceramics to the culture medium can be the reason for its desirable cell compatibility [75].

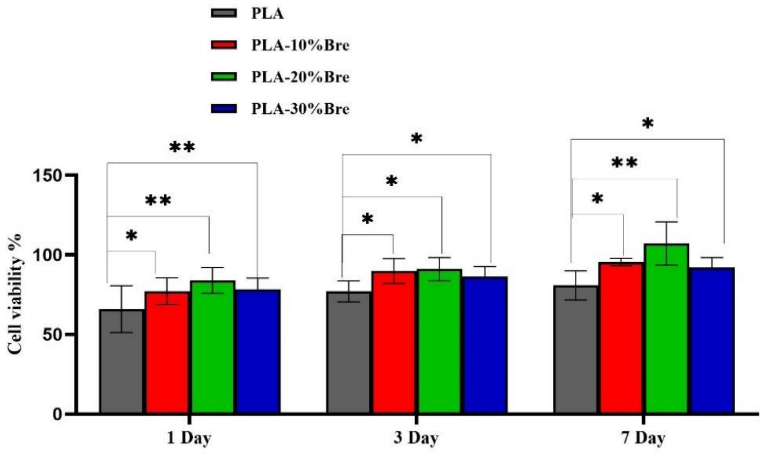

Fig. 11. The relative cell viability results with respect to the control sample on the 1, 3 and 7 days of cell culture related to the scaffolds containing (a) 0%, (b) 10 %, (c) 20 % and (d) 30 % of Bre; (*) $p < 0.05$, (**) $p < 0.01$.

3.9. Cells adhesion and proliferation assay

The images of cell adhesion and proliferation are shown in Fig. 12. As indicated, MG-63 cells interacted with all scaffolds. Increasing the amount of Bre powder led to more cell stretching and proliferation on the outer surface of the scaffold. The attachment and spreading of the MG-63 cells on the composite scaffolds was considerably improved compared to the pure PLA scaffold. Furthermore, increasing the amount of Bre powder in the composite scaffolds demonstrates the ability of Bre powder to promote cell growth and differentiation on the surface of composite scaffolds. According to the results, a poor cell adhesion and proliferation in the pure PLA scaffolds is a result of its hydrophobic nature. Addition of Bre powder improved cell spreading on the surface of scaffold possibly due to the formation of Si-OH groups and improved hydrophilicity of scaffolds. Some previous studies indicated that the silica groups in the ceramics containing Si ions provide negative charge groups of silanol because of the lower isoelectric point. Silanol groups with negative charges and low isoelectric point provide appropriate active binding sites for proteins during cell culture leading to improved cell proliferation and provide a desirable surface for cell growth [76]. The silanol groups of Bre ceramic can bind to different functional

ISSN 1019-6609
eISSN 1853-4961

groups, such as growth factors, and providing a favorable surface environment for cell growth and higher cellular activity [76]. Yi et al. [77] confirmed not only the release of calcium ions but also the release of Mg and Si ions from bredigite surface of scaffolds as essential nutrients for cell growth, which stimulate cell growth and differentiation, resulting in a higher proliferation rate. Therefore, the presence of Bre powder in the polymer-based composite scaffolds offers a suitable scaffold with appropriate biocompatibility.

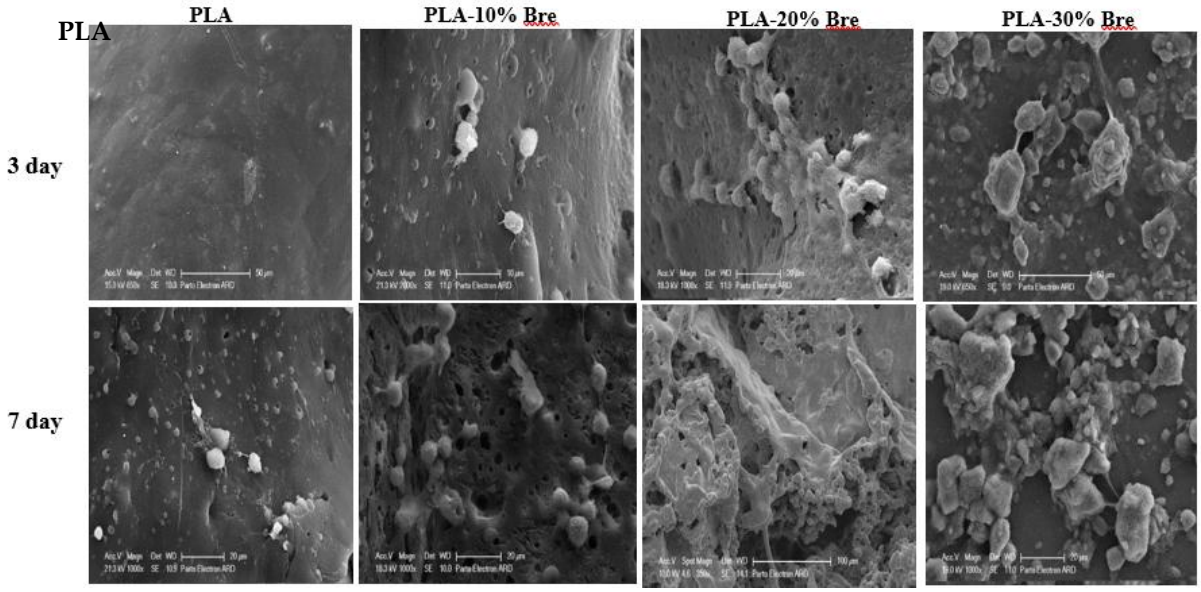

Fig.12. The viability of the MG63 cells grown on different PLA-Bre scaffolds after 3 and 7 days of culture (n ¼ 3) (*P < 0.05). b) SEM images of the MG63 cells seeded on pure PLA and nanocomposite PLA-Brescaffolds for 3 and 7 days.

3.10. Alizarin Red Assay

The Alizarin red assay is a distinct staining method used to evaluate calcium deposition on the surface of the extracellular matrix (ECM) [78]. This assay utilizes an organic compound that specifically stains (or identifies) mineralized components. Mineralization is a critical stage in the cell differentiation process of osteoblasts[79]. The absorbance intensity of the stained cell or tissue has a direct relationship with the minerals present in the ECM. This assay can investigate the scaffold's potential for bone tissue engineering and ECM deposition[78]. Calcium deposits on the scaffolds were evaluated on the 3rd and 7th days (Fig. 13). With the addition of Bre from 10% up to 30% by weight, enhanced calcium deposition was observed compared to the pure PLA scaffold and control sample. The scaffold containing 20% Bre showed significantly higher values compared to the others ($p < 0.001$). On the 7th day, the scaffolds containing 20% and 30% Bre exhibited significantly higher calcium deposits compared to other groups ($p < 0.001$). However, no significant differences were observed between the scaffolds containing 20% and 30% Bre on the 3rd and 7th days ($p > 0.05$).

PLA scaffolds coated with CaO-MgO-SiO_2-P_2O_5 based bioceramics have previously demonstrated significantly higher mineral mineralization compared to pure PLA [79]. This phenomenon can confirm the potential of akermanite in increasing the rate of cell differentiation [23]. The Si content in CaO-MgO-SiO_2 based bioceramic structures can create calcification sites, which leads to the mineralization of the matrix [72,80]. Furthermore, the presence of Bre-Ca structure can stimulate cell differentiation and increase the mineralization rate [81]. Based on these results, Bre powder has a positive effect on calcium deposition during cell differentiation

ISSN 1019-6609
eISSN 1853-4961

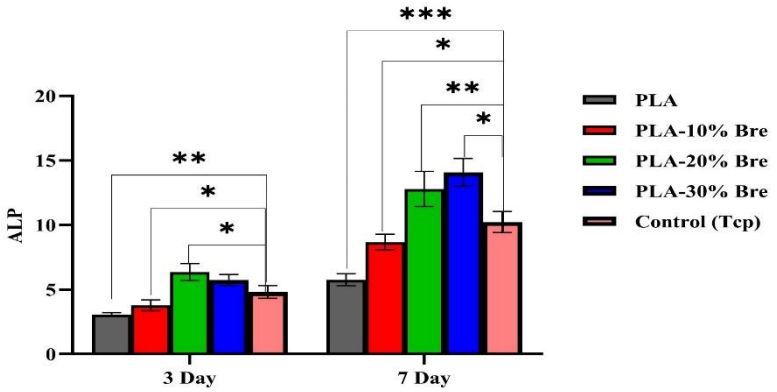

Fig 13. The colorimetric results of calcium staining obtained from the alizarin red assay related to the scaffolds containing (a) 0%, (b) 10 %, (c) 20 % and (d) 30 % of Bre on the 3 and 7 days. (*) $p < 0.05$, (**) $p < 0.01$ and (***) $p < 0.001$.

3.11. ALP assay

Alkaline phosphatase (ALP) is an active enzyme secreted by osteoblasts. It is also recognized as a suitable biomarker for osteoblast differentiation [78]. Figure. 14 illustrates the level of ALP expression for scaffolds containing varying amounts of Bre (from 0% to 30%) on the 7th day of cell culture. On the 7th day, scaffolds containing 20% and 30% Bre presented significantly higher ALP expression than the pure PLA scaffold ($p < 0.05$). Furthermore, a significantly higher ALP expression was observed in the scaffold containing 20% Bre compared to the one with 10% Bre on the 7th day ($p < 0.05$).

In addition, other studies have reported the positive effect of CaO-MgO-SiO_2-based bioceramics on ALP expression[82,72,83]. Specifically, electrospun PLA-based scaffolds containing CaO-MgO-SiO_2 bioceramics exhibited a significantly higher ALP level in comparison with the pure PLA scaffold[70]. Moreover, a study on polymeric sponge scaffolds reported that akermanite-containing scaffolds led to higher osteoblast differentiation compared to those lacking this bioceramic[83]. The presence of Si, Mg, and Ca in the Bre structure can increase cell activity, thereby elevating ALP activity[84]. These results indicate that Bre has a high potential to stimulate cell differentiation in bone tissue engineering applications.

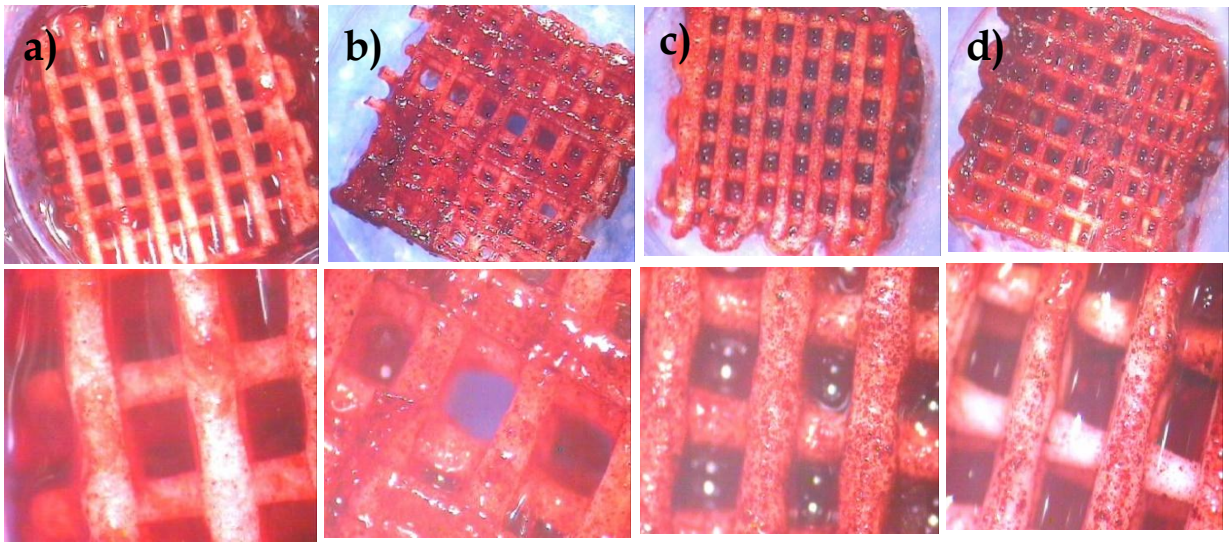

ISSN 1019-6609
eISSN 1853-4961

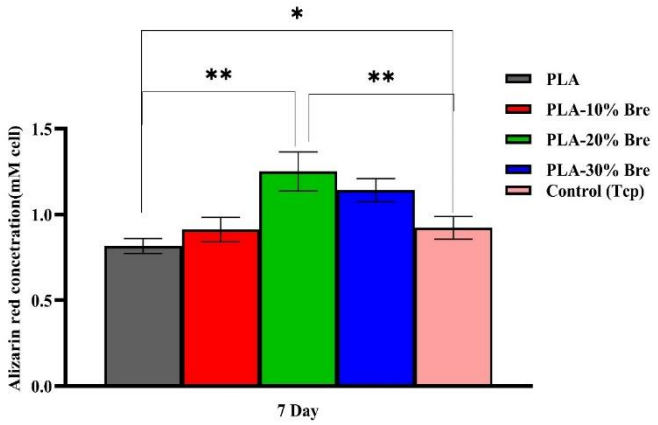

Fig 14. ALP activity assay results on the 3rd and 7th days of cell culture for the scaffolds containing (a) 0%, (b) 10 %, (c) 20 % and (d) 30 % of Bre; (*) $p < 0.05$, (**) $p < 0.01$ and (***) $p < 0.001$.

4.Conclusion

In this study, PLA based composite scaffolds with different Bre contents (0, 10, 20 and 30 wt.%) and porous gradient architectures were designed and fabricated by the FDM technology. The effect of porosity gradient and Bre nanoparticles was assessed on the mechanical and biological properties of the scaffolds. The addition of Bre powder to polymer matrix enhanced the compressive strength as well as the elastic modulus. Moreover, the presence of Bre particles in the scaffold improved the biodegradable and bioactive properties of the scaffolds. It was seen that the MG-63 cells were well attached, grown, and proliferated on the Bre-containing scaffolds. The cell viability increased during the cell culture over time on the scaffolds, as the content of Bre increased. Increasing the Bre content up to 30 wt.% led to a significant increase in calcium deposition compared to the pure PLA scaffold ($p < 0.001$). The results of ALP secretion on the 7th day for the scaffolds containing 20 % and 30 % of Bre was significantly higher than the pure PLA scaffold (0.05).

CRediT authorship contribution statement

Somayeh Mohammadi: Conceptualization, Methodology, Investigation, Formal analysis, Writing-Original draft, Writing-Review& Editing, Visualization. **Hamid Reza Rezaie**: Supervision, Resources, Editing. **Jafar Javadpour**: Supervision, Resources. **Mahshid Kharaziha**: Supervision, Resources, investigation, Editing. **Ali Reza Khavandi**: Supervision, Resources.

Declaration of competing interest

The authors declare that no funding was received for this research and they have no known competing financial interests or personal relationships that could have appeared to influence the work reported in this paper.

Data Availability Declaration

The datasets generated and/or analyzed during the current study are available from the corresponding author on reasonable request.

References

[1] P., Anne Marie, Ch., Sara, R., Hajar, et al. 2018. Mechanobiologically optimized 3D titanium-mesh scaffolds enhance bone regeneration in critical segmental defects in sheep. J. Sci. Trans. Med. 10

(eaam8828): 10.1126/scitranslmed.aam8828.
[2] L., Philipp, P., Hans Christoph, P., Tomas, K., Philipp, F., Horst. 2011. Scaffolds for bone healing: concepts, materials and evidence. J. Inj. 42: 569–573. https://doi.org/10.1016/j.injury.2011.03.033.
[3] L., Robert, Vacanti., Joseph P. 1993. Tissue engineering. J. Sci. 260: 920–926. http://doi: 10.1126/science.8493529.
[4] K., Gerry L, D., Mani, M., Antonios G. 2020. Materials design for bone-tissue engineering. J. Nat. Rev. Mater. 5: 584–603. https://doi.org/10.1038/s41578-020-0204-2.
[5] L., Yulin, X., Yin, L., Changsheng. 2017. The horizon of materiobiology: a perspective on material-guided cell behaviors and tissue engineering. J. Chem. Rev. 117: 4376–4421. http://doi: 10.1021/acs.chemrev.6b00654.
[6] Z., Parisa, A., Babak, K., Saeed, M., Mohammad Hussein. 2019. Preparation and characterization of poly ε-caprolactone-gelatin/multi-walled carbon nanotubes electrospun scaffolds for cartilage tissue engineering applications. Int. J. Polym. Mater. Polym. Biomater. 69: 1–12. https://doi.org/10.1080/00914037.2018.1563088.
[7] L., Andrea Di, L., Alessia, C., Giuseppe, M., Carlos, B., Clemens van, M., Lorenzo. 2016. Toward mimicking the bone structure:design of novel hierarchical scaffolds with a tailored radial porosity gradient. J. Biofabric. 8: 1-16. http://doi: 10.1088/1758-5090/8/4/045007.
[8] Q., Huawei, H., Zhenyu, Ch., Zhigang, T., Lan, G., Chongjian, L., Kaizheng, P., Haobo, F., Hongya, R., Changshun. 2021. Fractal Design Boosts Extrusion-Based 3D Printing of Bone-Mimicking Radial-Gradient Scaffolds. J. Res. Art. 2021: 1-13. https://doi.org/10.34133/2021/9892689.
[9] Hench, Larry L., Wilson., June. 1993. An Introduction to Bioceramics. World Scientific, London, UK.
[10] K., Samar Jyoti, B., Susmita, H., Howard L, B., Amit. 2003. Development of controlled porosity polymer-ceramic composite scaffolds via fused deposition modeling. Mater. Sci & Eng C. 23: 611-620. http://doi:10.1016/S0928-4931(03)00052-3.
[11] D., Y., M., Zhang, X., Chen, X., Pu, X., Liao, Z., Huang, et al. 2017. A novel akermanite/poly (lactic-co-glycolic acid) porous composite scaffold fabricated via a solvent castingparticulate leaching method improved by solvent selfproliferating process. Regenerat. Biomater. 4: 233-242. http://doi: 10.1093/rb/rbx014.
[12] N., S., B., M., F., E., K., M. 2017. Combination of PLA micro-fibers and PCL-gelatin nano-fibers for development of bone tissue engineering scaffolds. Int. J. Swarm. Intell. Evol. Comput. 6: 1-4. http://doi:10.4172/2090-4908.1000150.
[13] Nair, L. S., Laurencin, C. T. 2007. Biodegradable polymers as biomaterials. Prog. Polym. Sci. 32: 762-798. https://doi.org/10.1016/j.progpolymsci.2007.05.017.
[14] Askari, E., Naghib, S. M., Seyfoori, A., Javidi, M. A., Ansari, A. M. 2022. Highly bioactive Akermanite-Monticellite nanocomposites for bone tissue engineering: a tunable three-dimensional biological study. J. Mater. Res. Technol. 20: 4066-4076. https://doi.org/10.1016/j.jmrt.2022.08.136.
[15] Sopcak, T., Medvecky, L., Jevinova, P., Giretova, M., Mahun, A., Kobera, L., et al. 2023. Physico-chemical, mechanical and antibacterial properties of the boron modified biphasic larnite/bredigite cements for potential use in dentistry. J. Ceram. Int. 49: 6531-6544. https://doi.org/10.1016/j.ceramint.2022.10.119.
[16] Kaur, G., Kumar, V., Baino, F., Mauro, J. C., Pickrell, G., Evans, I., et al. 2019. Mechanical properties of bioactive glasses, ceramics, glassceramics and composites: state-of-the-art review and future challenges. Mater. Sci. Eng. C. 104: 1-14. https://doi.org/10.1016/j.msec.2019.109895.
[17] Wu, C., Chang, J. 2007. Synthesis and in vitro bioactivity of bredigite powders. J. Biomater. Appl. 21: 251-263. https://doi.org/10.1177/0885328206062360.
[18] Wu, C., Chang, J., Wang, J., Ni, S., Zhai, W. 2005. Preparation and characteristics of a calcium magnesium silicate (bredigite) bioactive ceramic. J. Biomater. 26: 2925-2931.

https://doi.org/10.1016/j.biomaterials.2004.09.019.
[19] Yi, D., Wu, C., Ma, B., Ji, H., Zheng, X. 2014. Chang J. Bioactive bredigite coating with improved bonding strength, rapid apatite mineralization and excellent cytocompatibility. J. Biomater. Appl. 28: 1343-1353. https://doi.org/10.1177/0885328213508165.
[20] Fahad, A., Raj, Sh., Vishnu, M., Kartik Mangudi, K., S. Satish. 2020. Microarchitected 3D printed poly lactic acid (PLA) nanocomposite scaffolds for biomedical applications. J. Mech. Behav. Biomed. Mater. 103: 1-9. https://doi.org/10.1016/j.jmbbm.2019.103576.
[21] Ch., Gang, Ch., Ning, W., Qi. 2019. Fabrication and properties of poly (vinyl alcohol)/β-tricalcium phosphate composite scaffolds via fused deposition modeling for bone tissue engineering. Compos. Sci. Technol. 172: 17–28. https://doi.org/10.1016/j.compscitech.2019.01.004.
[22] W., Wenzhao, Zh., Boqing, L., Mingxin, L., Jun, Zh., Chengyun, H., Yanlong, W., Li, W., Kefeng, Zh., Changchun, L., Lei, F., Yujiang, Zh., Xingdong. 2021. 3D printing of PLA/n-HA composite scaffolds with customized mechanical properties and biological functions for bone tissue engineering. 224: 1-12. https://doi.org/10.1016/j.compositesb.2021.109192.
[23] A., Masoud, Kh., Mohammad, A., Seyed Mohammad, N., Milad J. 2021. The in-vitro biological properties of 3D printed poly lactic acid/akermanite composite porous scaffold for bone tissue engineering. 27: 1-12. https://doi.org/10.1016/j.mtcomm.2021.102176.
[24] D., Xixi, L., Haiyan, Zh., Yanling, O., Long, C., Junkai, Ch., Jiang. 2016. The stimulation of osteogenic differentiation of embryoid bodies from human induced pluripotent stem cells by akermanite bioceramics. J. Mater. Chem. B. 4: 2369–2376. http://doi: 10.1039/x0xx00000x.
[25] E., Marjan, E., Rahmatollah, R., Kheyvan, Kh., Mahshid, V., Ali. 2016. Mechanical and cytotoxicity evaluation of nanostructured hydroxyapatite-bredigite scaffolds for bone regeneration. Mater. Sci. Eng. 68: 603–612. https://doi.org/10.1016/j.msec.2016.06.030.
[26] Kh., Mehdi, K., Seyed Farshid B., B., Mohammad Reza, S., Sara. 2023. A novel strategy for fast and facile synthesis of bioactive bredigite nanoparticles using microwave-assisted method. 25: 1735-1747. https://doi.org/10.1016/j.jmrt.2023.05.274.
[27] B., Frank B, F., Heinrich, S., K, Wilfried. 1994. Cellular and molecular biological events at the implant interface. J. Cran-Max. Surg. 22: 12-17. https://doi.org/10.1016/S1010-5182(05)80290-2.
[28] Zeta Potential of Colloids in Water and Waste Water. 1985. ASTM Standard D 4187-82, American Society for Testing and Materials.
[29] H., Zheng Ming, H., Chuang Long, Y., A. Yang, Y., Aizhao, Zh., Yanzhong, H., Xiao Jian, Y., Junlin, W., Qingsheng. 2007. Encapsulating drugs in biodegradable ultrafine fibers through co-axial electrospinning. J. Biomed. Mater. Res. A 77: 169–179. http://doi: 10.1002/jbm.a.30564.
[30] K., Tadash, T., Hiroaki. 2006. How useful is SBF in predicting in vivo bone bioactivity. Biomater. 27: 2907-2915. https://doi.org/10.1016/j.biomaterials.2006.01.017.
[31] P., Daniele, S., Annachiara, J., Swati, S., Liga, S., Kristīne S A, D., Kenny, G., Piergiorgio, M., Elena. 2020. 3D printed Sr-containing composite scaffolds: effect of structural design and material formulation towards new strategies for bone tissue engineering. Compos. Sci. Technol. 191: 1-10. https://doi.org/10.1016/j.compscitech.2020.108069.
[32] G., Carl A, G., W Grady, P., Alexandra, P., Darwin J. 2004. An Alizarin red-based assay of mineralization by adherent cells in culture: comparison with cetylpyridinium chloride extraction. Anal. Biochem. 329: 77–84. http://doi: 10.1016/j.ab.2004.02.002.
[33] I., Noriyuki Y, L., Geun Hyoung, T., Sukenari, T., Yoshikazu, K., Norimichi. 2004. Preparation of diopside with apatite-forming ability by sol–gel process using metal alkoxide and metal salts. Coll. Surf. B. Bio. inter. 33: 1-6. https://doi.org/10.1016/j.colsurfb.2003.07.004.
[34] M., Seyed Mehdi, T., Fariborz, E., Rahmatollah. 2012. Synthesis, characterization and formation mechanism of single-phase nanostructure bredigite powder. Mater. Sci. Eng. C. 32: 133-139.

https://doi.org/10.1016/j.msec.2011.10.007.
[35] T., Fariborz, E., Rahmatollah. 2011. Mechanism of nanostructure bredigite formation by mechanical activation with thermal treatment. Mater. Lett. 65: 2354-2356. https://doi.org/10.1016/j.matlet.2011.04.108.
[36] H., Masoud A., M., Fatollah, R., Mohammad, T., Ali Reza. Synthesis and characterization of nanocrystalline merwinite (Ca3Mg(SiO4)2) via sol–gel method. Ceram. Int. 37: 175-180. https://doi.org/10.1016/j.ceramint.2010.08.034.
[37] S., Ali, A., Babak, N., Zahra, K., Faramarz, A., Ali. 2007. A novel method to low temperature synthesis of nanocrystalline forsterite. Mater. Res. Bulletin. 42: 666–673. https://doi.org/10.1016/j.colsurfb.2003.07.004.
[38] I., Noriyuki Y, L., Geun Hyoung, T., Sukenari, T., Yoshikazu, K., Norimichi. 2004. Sintering behavior and apatite formation of diopside prepared by coprecipitation process. Coll. Surf. B: Bio. inter. 34: 239–245. https://doi.org/10.1016/j.colsurfb.2004.01.007.
[39] O., Masataki, K., Takashi, K., Mihoko, Y., Kimihiro. 2001. Manipulation of selective cell adhesion and growth by surface charges of electrically polarized hydroxyapatite. J. Bio. Mater. Res. 57: 366-373. https://doi.org/10.1002/1097-4636(20011205)57:3<366.
[40] Chia, Nia, T., Shuji, N., Shunsuke, T., Yoshiaki, Y., Kazuhito, O., Masataka. 2001. A New Approach to Enhancement of Bone Formation by Electrically Polarized Hydroxyapatite. J. Dent. Res. 80: 1925-1929. https://doi.org/10.1177/00220345010800101201.
[41] S., Ralf, K., Andreas, G., Macus, D., Oliver, M., Oliver, R., Dieter, S., Jamal M. 2009. A new biphasic osteoinductive calcium composite material with a negative Zeta potential for bone augmentation. Bio. Med. central. 13: 1-8. http://doi:10.1186/1746-160X-5-13.
[42] D., Ali M., M., Ahmad, S., Rasoul, F., Mohammad Hossein, G., Zahra, D., Alma U. 2011. Bioactive glass nanoparticles with negative zeta potential. J. Ceram. Inter. 37: 2311-2316. https://doi.org/10.1016/j.ceramint.2011.03.026.
[43] C.W. Macosko, Rheology: Principles, Measurements, and Applications, Wiley-VCH, 1994.
[44] H.A. Barnes, A handbook of elementary rheology, Aberystwyth: Institute of Non-Newtonian Fluid Mechanics, University of Wales, 2000.
[45] Y. Wang, X. Hu, Y. Zheng, L. Wei, Effect of filler content and aspect ratio on rheological and mechanical properties of poly (lactic acid)/hydroxyapatite composites, J. Appl. Polym. Sci. 133 (2016) 43105. https://doi.org/10.1002/app.43105
[46] A.V. Shenoy, Rheology of polymer composites: liquid crystal polymers, blends and multiscale materials, Elsevier, 1999.
[47] T.P. Mohan, K. Kanny, Review on rheological properties of natural fiber-reinforced polymer composites, J. Compos. Sci. 2 (2018) 52. https://doi.org/10.3390/jcs2030052.
[48] T.G. Mezger, The Rheology Handbook: For Users of Rotational and Oscillatory Rheometers, Vincentz Network GmbH & Co KG, 2011.
[48] C. Sammon, J. Yarwood, N. Everall, A study of the thermal degradation of poly(lactic acid) using FTIR spectroscopy and thermal analysis, Polym. Degrad. Stabil. 69 (2000) 1-13. https://doi.org/10.1016/S0141-3910(99)00067-1
[49] K.S. Anderson, K.M. Schreck, Thermal degradation of poly(lactic acid) and poly(lactic acid)-based biocomposites, in: Biodegradable Polymers and Polymer Composites, Springer, Berlin, Heidelberg, 2013, pp. 165-188. https://doi.org/10.1007/978-3-642-37837-1_7
[50] S. Xie, X. Liu, B. Liu, Y. Song, L. Yu, The effect of ceramic particle content on the rheological and mechanical properties of ceramic particle-reinforced polymer composites, Polymers 11 (2019) 1630. https://doi.org/10.3390/polym11101630
[51] G.I.G.A.L.N.S. [Please provide full author names from the paper], 2017, Effect of filler

agglomeration on the rheological properties of polymer composites, J. Ind. Eng. Chem. 49, 12-20. [You will need to find the DOI for this paper].
[52] S. Zhang, Y. Li, T. Wang, L. Zhang, P. Liu, The lubricating properties of different ceramic particles in polymer matrix composites, Tribology Int. 135 (2019) 237-246. https://doi.org/10.1016/j.triboint.2019.03.003
[53] K., Elena V, K., Alexander M, F., Willis, M., Victor N. 2001. Sorption of atmospheric carbon dioxide and structural changes of Ca and Mg silicate minerals during grinding: I. Diopside. Int. J. Miner. Process. 61: 273–288. https://doi.org/10.1016/S0301-7516(00)00035-1.
[54] Kh., Maliheh, J., Seyed Hassan, Z., Payam, B., Reza, H., Reza. 2017. Physical, morphological, and biological studies on PLA/n HA composite nanofibrous webs containing Equisetum arvense herbal extract for bone tissue engineering. J. Appl. Polym. Sci. 134: 1-10. http://doi: 10.1002/APP.45343.
[55] M.R.M. Rejab, K.A.N.B. Kamaruzaman, M.N. Harun, M.R.M.N. Rejab, A comprehensive review on the effect of synthetic filler materials on fiber-reinforced hybrid polymer composites, Mater. Today Proc. 46 (2021) 1708–1717. https://doi.org/10.1016/j.matpr.2021.03.208
[56] B-R., Hamid Reza, A., Mohsen, I., Ahmad Fauzi, A., Madzlan, H., Zhina, P., Erik, D., Mohammad Reza, Ch., Xiongbiao. 2019. Coating biodegradable magnesium alloys with electrospun poly-L-lactic acid-akermanite-doxycycline nanofibers for enhanced biocompatibility, antibacterial activity, and corrosion resistance. Surf. Coat. Technol. 377: 1-14. https://doi.org/10.1016/j.surfcoat.2019.124898.
[57] Miao, X., Sun, D. 2010. Graded/Gradient Porous Biomaterials. Materials. 3: 26-47.
[58] O.J. Rojas, T.L.L. Leong, R.A.P.L.H.P.K.H.C.P.J.G.L.A.K.R.A.K.S.M.F.C.R.A.C.A., Contact angles and wettability of cellulosic surfaces: A review of proposed mechanisms and test strategies, BioResources 7 (2) (2012) 2697-2747. https://doi.org/10.15376/biores.7.2.2697-2747

[59] R., Seyed Iman E., Kh., Saied N., L., Zufu, A., Richard, Z., Hala. 2010. The influence hydroxyapatite nanoparticles shape and size on the properties of biphasic calcium phosphate scaffolds coated with hydroxyapatite-PCL composites. Biomaterials. 31: 5498–5509. https://doi.org/10.1016/j.biomaterials.2010.03.058.

[60] Arastouei, M., Khodaei, M., Atyabi, S. M., Nodoushan, M. J. 2020. Poly lactic acid-akermanite composite scaffolds prepared by fused filament fabrication for bone tissue engineering. J. Mater. Res. Tech. 9: 4540-14548. https://doi.org/10.1016/j.jmrt.2020.10.036.
[61] SH., Tadashi, SH., Mitsuhiro, Y., Kouichi, M., Yohtaro. 2008. Influence of β-tricalcium phosphate dispersion on mechanical properties of hydroxyapatite ceramics. J. Ceram. Soc. J. pn. 116: 1002–1005. https://doi.org/10.2109/jcersj2.116.1002.
[62] N., Forough M., R., Mohammad, R., Hamid Reza B. 2021. SYNTHESIS AND EVALUATION OF MECHANICAL AND BIOACTIVE PROPERTIES OF β-TCP/BREDIGITE SCAFFOLD FOR BONE TISSUE ENGINEERING. J. Advan. Mater. Eng. 40: 95-97. http://doi: 10.47176/JAME.40.3.10534.
[63] W., Jie, Ch., Fangping, Sh., Jung W, H., Hua, D., Chenglong, S., Jiancan, L., Changsheng. 2009. Preparation and characterization of bioactive mesoporous wollastonite–Polycaprolactone composite scaffold. Biomater. 30: 1080–1088. http://doi: 10.1016/j.biomaterials.2008.10.046.
[64] N., Miguel, A., Carlos, H., Charles M, G., Maria Pau, E., Susan E, P., Ja Solar. 2006. Development of a Biodegradable Composite Scaffold for Bone Tissue Engineering: Physicochemical, Topographical, Mechanical, Degradation, and Biological Properties. Adv. Polym. Sci. 200: 209–231. http://doi: 10.1007/12_068.
[65] D., Mani, Kh., Mahshid, Gh., Mazaher. 2012. Preparation and characterization of polycaprolactone/forsterite nanocomposite porous scaffolds designed for bone tissue regeneration. Compos. Sci. Tech. 72: 716–723. http://dx.doi.org/10.1016/j.compscitech.2012.01.023.

[66] R., Judith A, B., Aldo R, H., Larry L, M., Veronique, G., Sandrine E, J., Robert J. 2002. Development and in vitro characterization of novel bioresorbable and bioactive composite materials based on poly lactide foams and Bioglass for tissue engineering applications. Biomater. 23: 3871–3878. https://doi.org/10.1016/S0142-9612(02)00131-X.
[67] K., Tadashi, K., Hyun Min, K., Masakazu. 2003. Novel bioactive materials with different mechanical properties. Biomater. 24: 2161–2175. https://doi.org/10.1016/S0142-9612(03)00044-9.
[68] Ch., Rajan, V., Jana, K., Genasan, R., Hanumantha Rao B., M., Malliga Raman, K., Tunku, S., Sasikumar, L., Janis. 2016. In-vitro bioactivity, biocompatibility and dissolution studies of diopside prepared from biowaste by using sol-gel combustion method. Mater. Sci. Eng. C. 68: 89–100. http://doi:10.1016/j.msec.2016.04.110.
[69] T., Cheng Ming, T., Yi Hung, H., Shan Hui. 2015. Poly(vinyl alcohol) Nanocomposites Reinforced with Bamboo Charcoal Nanoparticles: Mineralization Behavior and Characterization. Mater. (Basel). 8: 4895–911. http://doi:10.3390/ma8084895.
[70] R., Maryam, F., Mohammadhossein, A., Mehdi. 2018. Preparation and structural characterization of bioactive bredigite (Ca7MgSi4O16) nanopowder. J. Alloys. Compd. 732: 9–15. https://doi.org/10.1016/j.jallcom.2017.10.132.
[71] P., Juris, L., Dagnija, C., Liga B, L., Janis, L., Vitalijs. 2020. Release of anticancer drug doxorubicin from biodegradable polymer coated porous hydroxyapatite scaffolds. Adv. Mater. Res. 11: 328-355. https://doi.org/10.4028/www.scientific.net/AMR.284-286.1770.
[72] X., Lunguo, Y., Zhilan, M., Lixia, W., Xiuhui, L., Jiaqiang, J., Xinquan, Zh., Zhiyuan, L., Kaili, Ch., Jiang, F., Bing. 2016. Akermanite bioceramics promote osteogenesis, angiogenesis and suppress osteoclastogenesis for osteoporotic bone regeneration. Sci. Rep. 6: 1-17. http://doi: 10.1038/srep22005.
[73] N., Aliakbar, A., Majid, Gh., Hamid, S., Ali, Ch., Akbar, Kh., Amirsalar. 2017. A comparative study on the synthesis mechanism, bioactivity and mechanical properties of three silicate bioceramics. Mater. Sci. Eng. C. 72: 259–267. https://doi.org/10.1016/j.msec.2016.11.084.
[74] S., Saeed, Kh., Amirsalar S., S., Saeed S –., A., Mohammad. 2018. Vibrations of beam-type implants made of 3D printed bredigite-magnetite bio-nanocomposite scaffolds under axial compression. Appl. Commun. Simulat. Ceram. Int. 44: 11282–11291. https://doi.org/10.1016/j.ceramint.2018.03.173.
[75] B-R., Hamid Reza, A., Mohsen, I., Ahmad Fauzi, A., Madzlan, H., Zhina, P., Erik, D., Mohammadreza, Ch., Xiongbiao. 2019. Coating biodegradable magnesium alloys with electrospun poly-L-lactic acid-akermanite-doxycycline nanofibers for enhanced biocompatibility, antibacterial activity, and corrosion resistance. Surf. Coat. 377: 1-14. https://doi.org/10.1016/j.surfcoat.2019.124898.
[76] D., Mani, F., Mohammadhossein, Kh., Mahshid. 2011. Novel forsterite/polycaprolactone nanocomposite scaffold for tissue. Mater. Lett. 65: 1931-1934. https://doi.org/10.1016/j.matlet.2011.03.047.
[77] Y., Deliang, W., Chengtie, Ch., Jiang, Zh., Xuebin, J., Heng, M., Bing. 2014. Bioactive bredigite coating with improved bonding strength, rapid apatite mineralization and excellent cytocompatibility. J. Biomatr. App1. 28: 43-53. https://doi.org/10.1177/0885328213508165.
[78] S., Mansoureh, Kh., Mohammad Taghi, R., Mohammad, R., Hossein S. 2019. Incorporation of nanohydroxyapatite and vitamin D3 into electrospun PCL/gelatin scaffolds: the influence on the physical and chemical properties and cell behavior for bone tissue engineering. Polym. Adv. Technol. 29: 451–462. https://doi.org/10.1002/pat.4134.
[79] B., Ashkan, S., Ahmad, R., Mohammad, R., Shahram, B., Hassan, S., Fatemeh, S., Mansoureh, H-T., Sayed Ali. 2019. Electrophoretically deposited mesoporous magnesium silicate with ordered nanopores as an antibiotic-loaded coating on surface-modified titanium. Mater. Sci. Eng. 96: 765–775. https://doi.org/10.1016/j.msec.2018.12.013.
[80] R., Mohammad, B., Ashkan, S., Ahmad, R., Shahram. 2018. Gehlenite nanobioceramic: sol-gel

synthesis, characterization, and in vitro assessment of its bioactivity. Mater. Lett. 225: 89–92. https://doi.org/10.1016/j.matlet.2018.04.094.

[81] D., Xixi, L., Haiyan, Zh., Yanling, O., Long, C., Junkai, Ch., Jian. 2016. The stimulation of osteogenic differentiation of embryoid bodies from human induced pluripotent stem cells by akermanite bioceramics. J. Mater. Chem. B. 4: 2369–2376. http://doi: 10.1039/x0xx00000x.

[82] N., Atefeh, J., Ehsan S., S., Ali. 2017. Electrospun poly-L-lactic acid coated with silicate bioceramic nanoparticles enhance osteogenic differentiation of adipose tissue derived mesenchymal stem cells. J. Biomater. Tissue Eng. 7: 91–100. http://doi: 10.1166/jbt.2017.1544.

[83] Z-H., Azam, S-S., Samaneh, S-S., Saeed. 2016. The effective role of akermanite on the apatite-forming ability of gelatin scaffold as a bone graft substitute. Ceram. Int. 42: 17781–17791. https://doi.org/10.1016/j.ceramint.2016.08.106.

[84] S., Ali, B-R., Hamid Reza, K., Ebrahim, K-A, Masoud, Gh., Hamed. 2020. A study on the corrosion behavior and biological properties of polycaprolactone/bredigite composite coating on biodegradable Mg-Zn-Ca-GNP nanocomposite. Progress in Organic Coatings. 147: 1-14. https://doi.org/10.1016/j.porgcoat.2020.105822.